UPPSALA
UNIVERSITET

Digital Comprehensive Summaries of Uppsala Dissertations from the Faculty of Science and Technology 743

Multi-Electron Coincidence Studies of Atoms and Molecules

EGIL ANDERSSON

ACTA
UNIVERSITATIS
UPSALIENSIS
UPPSALA
2010

ISSN 1651-6214
ISBN 978-91-554-7805-6
urn:nbn:se:uu:diva-122811

Dissertation presented at Uppsala University to be publicly examined in Häggsalen, Ångströmlaboratoriet, Lägerhyddsvägen 1, Uppsala, Saturday, May 29, 2010 at 13:15 for the degree of Doctor of Philosophy. The examination will be conducted in English.

Abstract
Andersson, E. 2010. Multi-Electron Coincidence Studies of Atoms and Molecules. Acta Universitatis Upsaliensis. *Digital Comprehensive Summaries of Uppsala Dissertations from the Faculty of Science and Technology* 743. 71 pp. Uppsala. ISBN 978-91-554-7805-6.

This thesis concerns multi-ionization coincidence measurements of atoms and small molecules using a magnetic bottle time-of-flight (TOF) spectrometer designed for multi-electron coincidence studies. Also, a time-of-flight mass spectrometer has been used together with the TOF electron spectrometer for electron-ion coincidence measurements. The multi-ionization processes have been studied by employing a pulsed discharge lamp in the vacuum ultraviolet spectral region and synchrotron radiation in the soft X-ray region. The designs of the spectrometers are described in some detail, and several timing schemes suitable for the light sources mentioned above are presented.

Studies have been performed on krypton, molecular oxygen, carbon disulfide and a series of alcohol molecules. For the latter, double ionization spectra have been recorded and new information has been obtained on the dicationic states. A recently found rule-of-thumb and quantum chemical calculations have been used to quantify the effective distance of the two vacancies in the dications of these molecules.

For Kr, O_2, and CS_2, single-photon core-valence spectra have been obtained at the synchrotron radiation facility BESSY II in Berlin and interpreted on the basis of quantum chemical calculations. These spectra show a remarkable similarity to conventional valence photoelectron spectra.

Spectra of triply charged ions were recorded, also at BESSY II, for Kr and CS_2 by measuring, in coincidence, all three electrons ejected. The complex transition channels leading to tricationic states were mapped in substantial detail for Kr. It was found that for 3d-ionized krypton, the tricationic states are dominantly populated by cascade Auger decays via distinct intermediate states whose energies have been determined. The triple ionization spectra of CS_2 from the direct double Auger effect via S2p, S2s and C1s hole states contain several resolved features and show selectivity based on the initial charge localisation and on the identity of the initial state.

Keywords: multi-ionization, electron emission, time-of-flight spectroscopy, coincidence spectroscopy, core-valence ionization, synchrotron radiation, electron correlation

Egil Andersson, Department of Physics and Astronomy, Soft X-Ray Physics, Box 516, Uppsala University, SE-751 20 Uppsala, Sweden

ISSN 1651-6214
ISBN 978-91-554-7805-6
urn:nbn:se:uu:diva-122811 (http://urn.kb.se/resolve?urn=urn:nbn:se:uu:diva-122811)

Till Hania och Tobbe

List of Papers

This thesis is based on the following papers, which are referred to in the text by their Roman numerals.

I **Multi-electron coincidence study of the double Auger decay of 3d ionised krypton**
E. Andersson, S. Fritzsche, P. Linusson, L. Hedin, J. H. D. Eland, J.-E. Rubensson, L. Karlsson and R. Feifel
Submitted to *Physical Review A*.

II **Formation of Kr^{3+} via core-valence doubly ionised intermediate states**
E. Andersson, S. Fritzsche, L. Hedin, P. Linusson, J. H. D. Eland, L. Karlsson, J.-E. Rubensson and R. Feifel
In manuscript.

III **Double photoionization of alcohol molecules**
P. Linusson, M. Stenrup, Å. Larson, E. Andersson, F. Heijkenskjöld, P. Andersson, J. H. D. Eland, L. Karlsson, J.-E. Rubensson and R. Feifel
Physical Review A, vol. 80, num. 3, pp. 032516 1-6 (2009).

IV **Single-photon core-valence double ionization of molecular oxygen**
E. Andersson, M. Stenrup, J. H. D. Eland, L. Hedin, M. Berglund, L. Karlsson, Å. Larson, H. Ågren, J.-E. Rubensson and R. Feifel
Physical Review A, vol. 78, num. 2, pp. 023409 1-5 (2008).

V **Core-valence double photoionisation of the CS_2 molecule**
E. Andersson, N. Niskanen, L. Hedin, J. H. D. Eland, P. Linusson, L. Karlsson, J.-E. Rubensson, V. Carravetta, H. Ågren and R. Feifel
Submitted to *The Journal of Chemical Physics*.

VI **Spectra of the triply charged ion CS_2^{3+} and selectivity in molecular Auger effects**
J.H.D. Eland, C.F. Rigby, E. Andersson, J. Palauxdoux, L. Andric, F. Penent, P. Linusson, L. Hedin, L. Karlsson, J.-E. Rubensson, Y, Hikosaka, K. Ito, P. Lablanquie and R. Feifel
The Journal of Chemical Physics, vol. 132, pp. 104311 1-8 (2010).

The following is a list of papers to which I have contributed, but which are not included in the thesis.

- **Photoinduced formation of N_2 molecules in ammonium compounds**
  E. F. Aziz, J. Gråsjö, J. Forsberg, E. Andersson, J. Söderström, L. Duda, W. Zhang, J. Yang, S. Eisebitt, C. Bergström, Y. Luo, J. Nordgren, W. Eberhardt and J.-E. Rubensson
  The Journal of Physical Chemistry A, vol. 111, num. 39, pp. 9662–9 (2007).
- **Double photoionization of thiophene and bromine-substituted thiophenes**
  P. Linusson, L. Storchi, F. Heijkenskjöld, E. Andersson, M. Elshakre, B. Pfeifer, M. Colombet, J. H. D. Eland, L. Karlsson, J.-E. Rubensson, F. Tarantelli and R. Feifel
  The Journal of Chemical Physics, vol. 129, pp. 234303 1-8 (2008).
- **Coincidence technique using synchrotron radiation for triple photoionization: Results on rare gas atoms**
  J.H.D. Eland, P. Linusson, L. Hedin, E. Andersson, J.-E. Rubensson and R. Feifel
  Physical Review A, vol. 78, num. 6, pp. 063423 1-6 (2008).
- **Electronic Structure of Water Molecules Confined in a Micelle Lattice**
  J. Gråsjö, E. Andersson, J. Forsberg, E. F. Aziz, B. Brena, C. Johansson, J. Nordgren, L. Duda, J. Andersson, F. Hennies, J.-E. Rubensson and P. Hansson
  The Journal of Physical Chemistry B, vol. 113, num. 24, pp. 8201–5 (2009).
- **Local Electronic Structure of Functional Groups in Glycine As Anion, Zwitterion, and Cation in Aqueous Solution**
  J. Gråsjö, E. Andersson, J. Forsberg, L. Duda, E. Henke, W. Pokapanich, O. Björneholm, J. Andersson, A. Pietzsch, F. Hennies and J.-E. Rubensson
  The Journal of Physical Chemistry B, vol. 113, num. 49, pp. 16002–6 (2009).
- **Triple ionisation of methane by double Auger and related pathways**
  J.H.D. Eland, P. Linusson, L. Hedin, E. Andersson, J.-E. Rubensson and R. Feifel
  Chemical Physics Letters, vol. 485, issues 1-3, pp. 21-22 (2010).
- **Triple ionization spectra by coincidence measurements of double Auger decay: The case of OCS**
  J.H.D. Eland, M. Hochlaf, P. Linusson, E. Andersson, L. Hedin and R. Feifel
  The Journal of Chemical Physics, vol. 132, num. 1, pp. 014311 1-9 (2010).

Comments on my participation

Experimental physics, and particularly when carried out at large synchrotron radiation facilities, is intrinsically a collaborative effort. I have contributed in various ways, and to a varied extent, to the papers presented in this thesis. I took part in the experiments leading to all of the presented papers and I have taken the main responsibilty for the preparation and finalization of papers I, II, IV and V. My main contribution has been to develop software for analysing multi-coincidence time-of-flight data, and I have used these programs to perform the data analyses of the papers mentioned above.

Contents

1 Introduction 11
1.1 Historic background 11
1.1.1 Atoms and molecules 11
1.1.2 The electromagnetic spectrum 12
1.1.3 Spectroscopy 13
1.1.4 Atomic orbitals 14
1.2 Electronic transitions 15
1.3 Excitation and ionization 16
1.4 Decay mechanisms 17
1.4.1 Radiative decay 18
1.4.2 Auger decay 19
1.4.3 Multiple ionization 20
1.5 Visualization of transitions 20
2 Multiple ionization of atoms and molecules 25
2.1 Background 25
2.2 Single photon double ionization 26
2.2.1 Valence-valence ionization 26
2.2.2 Core-valence ionization 28
3 Experimental techniques 29
3.1 Coincidence spectroscopy 29
3.1.1 Coincidence statistics 30
3.2 Light sources 31
3.2.1 A pulsed He lamp 31
3.2.2 Synchrotrons 32
3.2.3 Monochromators 35
3.3 Experimental setup 36
3.3.1 The magnetic bottle time-of-flight-spectrometer 36
3.3.2 Timing 38
3.3.3 Time to energy conversion 39
3.3.4 The ion time-of-flight setup 40
4 Summary of papers 43
4.1 Papers I and II:
Creation of triply charged krypton via several ionization pathways 43
4.1.1 Experimental details 43
4.1.2 Results and discussion 45

4.2 Paper III:
Double photoionization of alcohol molecules 47
4.3 Paper IV and V:
Core-valence double photoionization of O_2 and CS_2 49
4.4 Paper VI:
Spectra of the triply charged ion CS_2^{3+} and selectivity in molecular Auger effects 52
4.4.1 Experimental details 52
4.4.2 Results 55
5 Outlook 59
6 Sammanfattning på svenska 61
7 Acknowledgements 63
8 Credits 65
Bibliography 67

1. Introduction

Correlated many-particle dynamics in Coulombic systems is one of today's grand challenges in physics. Multi-ionization studies on atoms and molecules provide information on the correlation between the electrons and also on the dynamics of the ionization processes. These mechanisms are highly relevant with regard to the ion and excited-state balance in the Earth's outer atmosphere and in astrophysical contexts, and such studies can be used to test current atomic and molecular structure theories to their limits. An improved understanding of ionization mechanisms in simple systems is most desirable in order to model the interaction of highly intensive ultraviolet and x-ray radiation in more complicated reactions, involving surface and bulk materials or biological samples.

In this chapter I will introduce some basic concepts in the field of atomic and molecular physics. The intention is to give readers who are unfamiliar with the subject some insight into the fundamental concepts, such as orbitals and common electronic transitions, and hopefully make it easier to follow the discussion in the other chapters. Undoubtedly, anyone with a background in this field will find this chapter very elementary. These readers can safely jump directly to chapter 2 for an introduction to multi-ionization of atoms and molecules, the theme of this thesis. The experimental techniques we have used are discussed in chapter 3 and the results of the measurements are summarized in chapter 4.

1.1 Historic background

1.1.1 Atoms and molecules

Two hundred years ago, John Dalton developed an atomic theory based on the idea that chemical substances are composed of small indivisible objects which combine in simple proportions, i.e. ratios of small integer numbers [1, 2]. Dalton's work [3] was based on the previous observation by Antoine Lavoisier [4] that the total mass in a chemical reaction remains constant, and Joseph Louis Proust's 'law of definite proportions' which states that all samples of a given chemical compound always have the same elemental composition.[1] During the 19th century many new elements were discovered and some physical prop-

[1] Like many other 'laws' presented in this chapter, the law of definite proportions is a simplification. Non-stoichiometric compounds, such as cuprates, are exceptions to this rule.

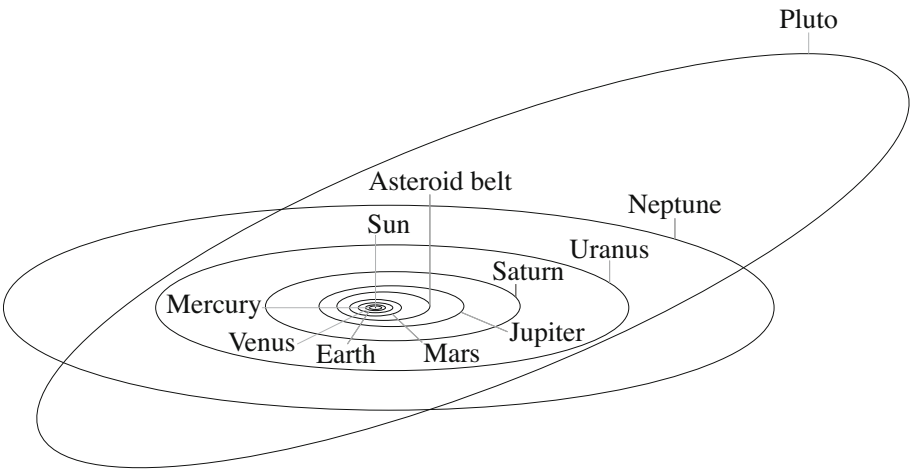

Figure 1.1: The solar system. The Bohr model of the atomic orbitals is based on similar concepts.

erties, such as 'heat' and 'light', which previously were thought to be chemical elements, were explained by other theories. However, it was not until 1897 that Joseph John Thomson discovered the electron [5] and concluded that the atom wasn't indivisible at all. Later on, experiments by Hans Geiger, Ernest Marsden and Ernest Rutherford showed [6] that most of the mass of the atom is located in a small nucleus in its centre.

1.1.2 The electromagnetic spectrum

Classic theories describe light as waves characterised by their amplitude and wavelength. This model explains a number of the properties of light, such as colour (different wavelengths), refraction (e.g. in lenses) and diffraction (see below and section 3.2.3). Eventually it was understood that light is connected to electricity and magnetism and can be described as changes in the electric and magnetic fields — electromagnetic waves. The term electromagnetic radiation covers many types of radiation which can be described by the same formalism as visible light. From the physicist's point of view, radio-waves and x-rays are just different aspects of electromagnetic radiation, interacting with matter in differing ways depending on the wavelength of the radiation. Ionizing radiation refers to any kind of radiation that is energetic enough to remove an electron from a sample. Ultraviolet radiation and x-rays are examples of electromagnetic radiation with this property. In the experiments presented in this thesis, vacuum ultraviolet (VUV) and soft x-rays have been used. These terms designate electromagnetic radiation in the energy range between ultraviolet and hard x-rays and have the common property that they are absorbed, i.e. stopped, by the atmosphere. In what follows, the term *light* will often be

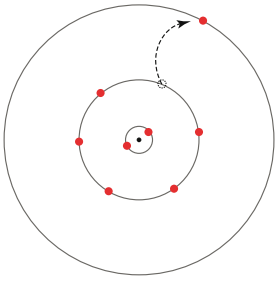

Figure 1.2: The Bohr model of the atom. The electrons orbit the central nucleus in circular trajectories at fixed distances. The arrow shows an excitation process where an electron has moved to an orbital further away from the nucleus.

used when referring to both vacuum ultraviolet and soft x-ray radiation, even though both these types of radiation are more energetic than light in the visible spectral region.

1.1.3 Spectroscopy

Spectroscopy originally designated the process of dispersing visible light into a spectrum of different wavelengths (or colours) e.g. by using a prism. This method was used to study various light sources, such as flames and the Sun. Another way of dispersing light is to use a grating (see also section 3.2.3). Optical spectroscopy based on gratings was pioneered by Joseph von Fraunhofer, who manufacured his own gratings to study the solar spectrum, and by Henry Augustus Rowland who invented the concave reflection grating, a device of great value to modern spectroscopists since it can be used to focus and diffract light using only one reflection. The term spectroscopy is nowadays used in many fields where one studies how the intensity of one physical property varies as a function of for example frequency, energy or mass. One example is electron spectroscopy, which is based on measuring the kinetic energy distributions of electrons released in an ionization event. Optical spectra of many samples display characteristic line patterns which depend on the composition of the sample. Fraunhofer studied the dark absorption lines in the spectrum of the Sun, and it was later realized that these lines could be explained in terms of the movement of the electrons in the atoms in the upper layers of the Sun. For the physicists of the early twentieth century, one of the great challenges was to create a model of the atom that could explain the lines in atomic spectra. A crucial step was Einstein's theory of light. Until then, light had been modelled as a wave, and the intensity of the light as the amplitude of the wave. Einstein postulated that light consists of small particles called photons. Each photon carries a definite amount of energy and interacts with matter individually. This concept was used to explain why a single x-ray photon, which has a comparatively high energy, can remove an electron from

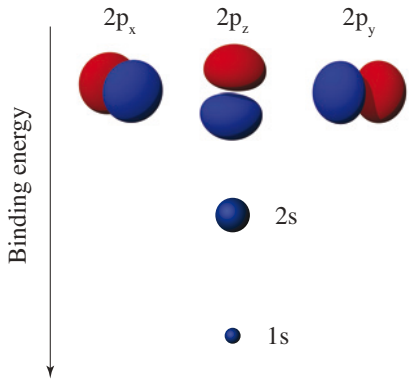

Figure 1.3: Atomic orbitals.

a sample, whereas a beam of visible light consisting of many photons with lower energy cannot remove any electrons.[2]

1.1.4 Atomic orbitals

Rutherford's observation that the atom consists of a small dense nucleus surrounded by electrons, and the discrete lines observed in optical spectra led Niels Bohr to develop a model of the atom resembling the solar system (depicted in figure 1.1). In the Bohr model (see figure 1.2), the electron is pictured as a small negatively charged particle orbiting the stationary, positively charged nucleus in the same manner as the planets orbit the Sun. In contrast to the solar system, only certain electron orbitals (characterized by their radii) are allowed, and the electrons can change orbital by interacting with electromagnetic radiation. This quantization of possible orbitals was later interpreted by Louis de Broglie as a consequence of the wave-particle duality of quantum physics; only those orbitals where the electron can be described as a standing wave are permitted. Although Bohr's model was too simple to explain many contemporary experimental findings, it is still useful for the discussion of electronic transitions. A simple example is excitation. In this process the atom absorbs the energy from an exciting source, e.g. a photon, by promoting an electron (or several electrons) to an orbital that lies further away from the nucleus.

Later on, the theory of quantum mechanics was developed by Heisenberg, Bohm, Schrödinger and many others, which resulted in more sophisticated models of the atomic orbitals. By using a wave description of the electron and solving the equations of motion, they found discrete orbitals, and the square

[2] At least not using lightsources available in the early twentieth century. Modern lasers can provide light that is sufficiently intense to cause non-linear effects, where several photons are absorbed simultaneously.

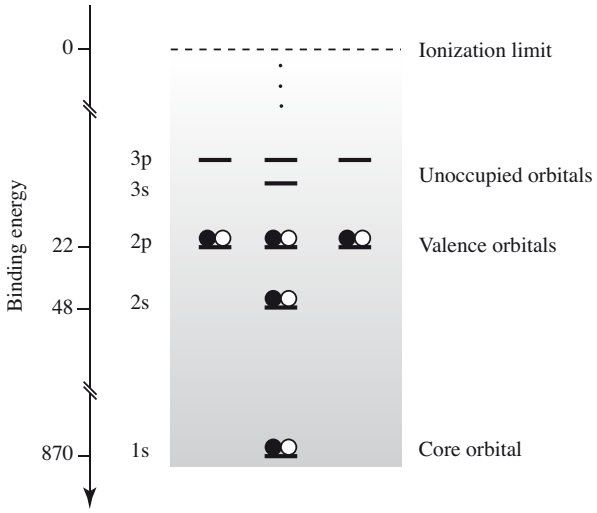

Figure 1.4: Schematic illustration of the orbitals of the neon atom. Neon has in total ten electrons, which, in the ground state, occupy the orbitals 1s, 2s and 2p.

of the wavefunction describing such an orbital can be interpreted as the probability distribution of finding an electron at a certain position. An illustration of such orbitals is shown in figure 1.3.

1.2 Electronic transitions

Optical and electron spectroscopy are powerful tools for investigating atoms and molecules in detail, since they provide a probe into the electronic structure of the sample. In contrast to classical mechanics, where many physical properties can be measured directly, without significantly affecting the sample, quantum mechanical systems, such as an atom, can not be studied without disturbing them.[3] Quite often it is the dynamics of the reaction to an initial perturbation that interests the researcher. The study of atoms and molecules thus requires experimental equipment designed to disturb the system and to observe the response. In the experiments presented in this thesis, the perturbation consists of changing the electronic state by adding energy to the sample.

[3]Landau and Lifshitz puts it this way in their volume on quantum mechanics [7] p. 3: "The measuring process has in quantum mechanics a very important property: it always affects the electron subjected to it and it is in principle impossible to make its effect arbitrarily small, for a given accuracy of measurement. The more exact the measurement, the stronger the effect exerted by it, and only in measurements of very low accuracy can the effect on the measured object be small".

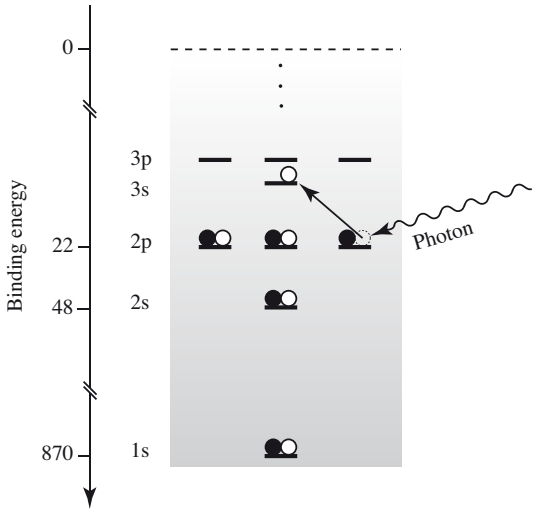

Figure 1.5: Photoexcitation of neon. A photon of an energy that equals the energy difference between the neutral ground state and the 2p → 3s excited state is absorbed, leading to a single electron excitation.

This has been achieved by irradiating the samples with photons in the vacuum ultraviolet and x-ray spectral regions, a procedure which can lead to either electronic excitation or the removal of one or more electron(s). The latter process is called *ionization*.

1.3 Excitation and ionization

Excitation and ionization can be visualized using diagrams of the orbital energies. Figure 1.4 shows the orbitals of a neon atom in its neutral ground state, which is the electronic state of the lowest total energy. One can think of the diagram as a 'well' where the electrons occupy various orbitals at different depths which represents the energy level of the orbital. The low-lying orbitals are referred to as *core* or *inner shell* orbitals and the outermost orbitals are called *valence* orbitals. Each orbital only has room for a certain number of electrons, which is a consequence of the Pauli exclusion principle.[4] For further reading see e.g. Richard Feynman's Lectures on physics [9].

[4]The Pauli exclusion principle states that two identical fermions, e.g. electrons, cannot occupy the same quantum state simultaneously [8]. '[T]he total wave function [of two identical fermions is] completely anti-symmetric [with respect to exchanging their coordinates]' [5].

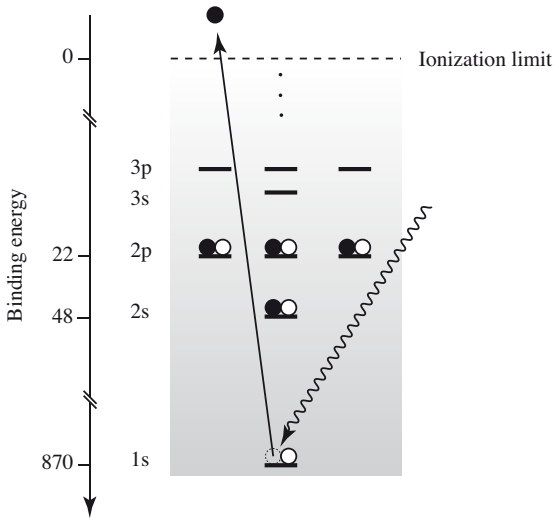

Figure 1.6: Photoionization of neon. A Ne^+ ion with a 'core hole in 1s' is created when a high energy photon is absorbed and an electron is ejected from the 1s orbital.

In order to move an electron from one orbital to one that lies further up in the figure, some energy must be provided; long vertical distances in the figure translate into more energy.

The excitation process is visualized in figure 1.5. Absorption of a photon can only lead to excitation if the photon energy equals the energy difference between the two states involved.[5] Photoionization occurs if the photon energy is large enough to 'lift' the electron over the edge of the 'well' (indicated by the dashed line in figure 1.6). The minimum energy required to remove an electron from the atom is referred to as the binding, or ionization, energy. It is indicated on the 'Binding energy' scale to the left in the figure. In electron spectroscopy, energies are often given in the unit electronvolts, eV, which is defined as the kinetic energy of an unbound electron after beeing accelerated from rest by a potential difference of 1 volt.

1.4 Decay mechanisms

An excitation or ionization process often leaves the system in an excited state. Excited electronic states are unstable, since the system tends to decay to states with lower total energy (not to be confused with the binding energy of an electron) until it has reached the state with the lowest possible energy. The

[5]There are several physical properties, such as angular momentum, that must be conserved which give rise to additional 'selection rules'.

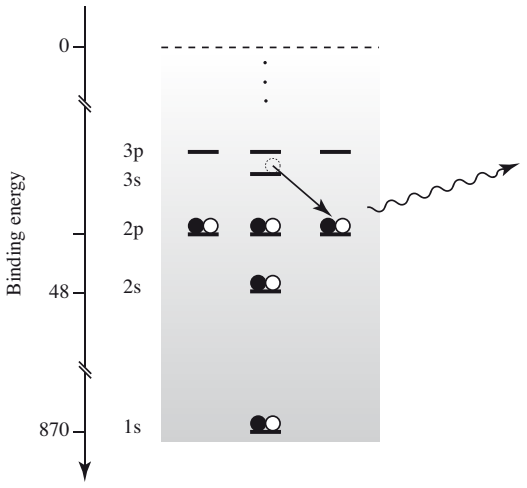

Figure 1.7: Schematic illustration of radiative decay. The excited neon atom returns to its ground state by emitting a photon. The process is the reverse of the photoabsorption illustrated in figure 1.5 and the photons in the two figures have the same wavelength.

surplus energy can be emitted from the system as a photon or an electron. Within the framework of this thesis, the excitation/ionization and the decay to a lower state can usually be considered as separate processes.

1.4.1 Radiative decay

Let us consider a simple two-step process, where the system first is excited by absorbing a photon of a certain wavelength and then decays back to the ground state by emitting a photon of the same wavelength (cf. figure 1.7). The overall effect of the described two-step process is essentially that the photon has bounced (scattered elastically), but there are many other possible radiative transitions. There are in fact several spectroscopic techniques devoted to the detection of photons emitted in such processes. However, since the spectroscopic method used in the experiments presented in this thesis is insensitive to photons, radiative decays will not be discussed further. Such decays might nevertheless play a role indirectly, if they would compete with other decay mechanisms which can be detected by the spectrometer. It may be noted that radiative decay does not necessarily take the system to its ground state in a single step. In many practical applications, e.g. lasers, phosphorescent ('afterglow') pigments and fluorescent markers (such as the green fluorescent protein used in microscopy), the colour of the emitted light is different from the colour of the light used for excitation.

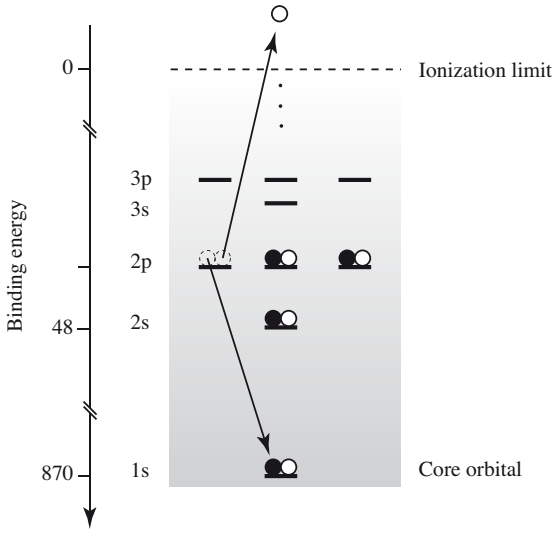

Figure 1.8: Schematic example of an Auger decay. The energy released when the core hole in 1s is 'filled' by an electron from 2p is transferred to another electron in the 2p orbital, which is ejected.

1.4.2 Auger decay

An excited atom can also decay to a state with lower energy by emitting an electron. This phenomenon was discovered independently by Lise Meitner [10] and Pierre Auger [11] and is a very common decay process for core hole states in the lighter element of the periodic table. An example of this process, referred to as 'Auger decay', is shown in figure 1.8. When an electron from the 2p orbital fills the 1s orbital the atom lowers its energy. This energy can either be released in the form of a photon, as described in the previous section,[6] or be transferred to another electron, which will be ejected if the energy is large enough.

In the systems relevant for this thesis, the energy difference between the inner orbitals is quite large, and Auger decays often dominate over radiative decays. The kinetic energy of the Auger electron depends on the energy difference between the two states involved in the decay, and this is a characteristic property of each atom or molecule. In addition, it is independent of the method used for creating the initial core hole. These properties has made Auger spectroscopy a widely used technique, see e.g. Ref. [12].

[6]Only some radiative transitions are allowed because of the selection rules mentioned in the context of photoexcitation.

Double Auger decays

An effect of Auger decay is that while the initial vacancy is filled by an electron a new hole is created in a less energetic orbital. Sometimes, this newly created state may undergo a second Auger decay. Such a process is referred to as an Auger cascade and can occur in several steps, where one electron is emitted in each step, and the atom ends up in a multiply ionized final state. It may also happen that two Auger electrons are emitted in a single step [13], which is referred to as direct double Auger. Paper I concerns the Auger decay of core-ionized krypton, and an example of cascade Auger decays is illustrated in figures 4.2 and 4.4 in section 4.1.

1.4.3 Multiple ionization

In the experiments presented in this thesis, we have made coincidence measurements of several electrons, and –sometimes– ions. For instance, we have studied double ionization processes where the absorption of a single photon leads to the emission of two electrons. The emission of the two electrons can be the result of a direct process where two electrons are ejected simultaneously, or an indirect process, i.e. an inner shell ionization followed by Auger decay. The coincidence method used and multi-ionization processes will be discussed in detail in the following chapters.

The resulting coincidence data sets can be presented as two-dimensional histograms where the detected coincidence events are binned with respect to the kinetic energy of the electrons. These histograms are often referred to as *coincidence maps*, since they display the intensity, or frequency in the histogram, as a function of two variables, i.e. the kinetic energy of each of the two electrons detected in double ionization. A few simple examples are presented in the next section.

1.5 Visualization of transitions: Energy diagrams and coincidence maps

It is often helpful to illustrate the processes discussed above using energy diagrams. An example diagram for a hypothetical system X is shown in figure 1.9, where the energy levels of each charge state of X is plotted in a separate column with the neutral system to the left, the singly charged ion X^+ in the middle column and the doubly charged ion X^{2+} in the right column. The energy levels in this diagram refer to the total energy of the system and should not be confused with binding energies such as the ones shown in figure 1.8. The values of the energy levels are related to the neutral unexcited ground state, which defines the zero of the energy scale.

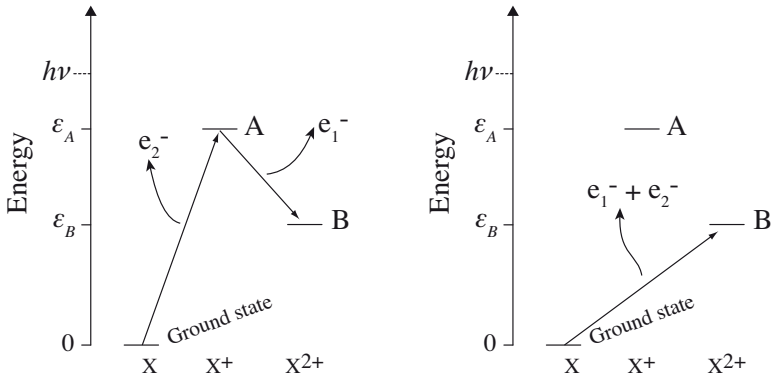

Figure 1.9: Energy level diagram illustrating double ionization processes of a hypothetical system X. The left panel shows a two-step process where the system is first ionized by an x-ray photon with energy $h\nu$ (indicated on the y-axis) to the state A of the X^+ ion. The ion then decays to the state B of X^{2+} by emitting an Auger electron. The electrons are numbered according to their kinetic energies. In this example $\varepsilon_1^{\mathrm{Aug}} > \varepsilon_2^{\mathrm{ph}}$. The right panel shows direct double photo-ionization to the state B of X^{2+} where two electrons are emitted simultaneously and share the available kinetic energy between themselves.

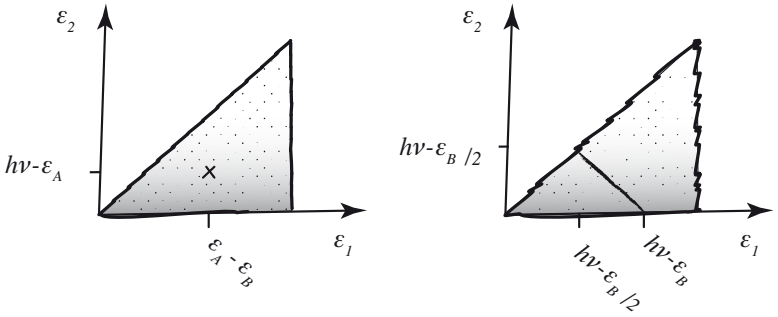

Figure 1.10: Schematic illustration of coincidence maps corresponding to the double ionization processes depicted in figure 1.9. The maps show the number of detected two-electron coincidence events as function of the kinetic energy of the fastest electron ε_1, (x-axis) and of the slowest electron ε_2 (y-axis). The left map corresponds to the two-step process shown in the left panel of figure 1.9. In this process two electrons with fixed energies are emitted which results in a single dot in the coincidence map. The right coincidence map corresponds to direct double ionization (illustrated in the right panel of figure 1.9). The two electrons share the kinetic energy between themselves, which results in a line in the coincidence map described by $\varepsilon_2 = h\nu - \varepsilon_B - \varepsilon_1, \quad \varepsilon_2 < \varepsilon_1$.

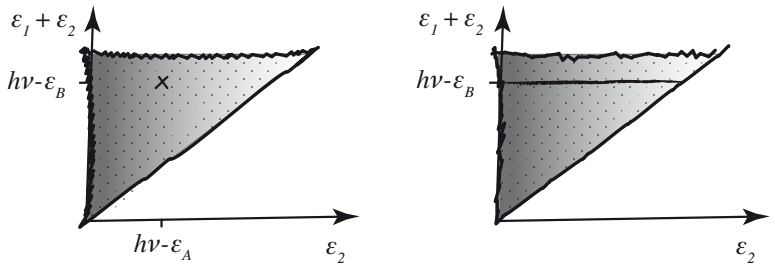

Figure 1.11: Coincidence maps of double ionization. By plotting the coincidence data displayed in figure 1.10 with the total kinetic energy, $\varepsilon_1 + \varepsilon_2$, on the *y*-axis and the kinetic energy of the slow electron, ε_2, on the *x*-axis it is easy to see that the line in the right panel corresponds to an electronic transition where $\varepsilon_1 + \varepsilon_2$ is constant.

The left panel of figure 1.9 shows the energy diagram representation of a photoionization event were initially one electron is removed. The final state of the first ionization event is labelled A, and the energy relative to the ground state of X is ε_A. If a photon energy of $h\nu$ is used, the emitted photoelectron will have an energy of $\varepsilon^{\mathrm{ph}} = h\nu - \varepsilon_A$. It is clear that if we increase the photon energy, the kinetic energy of the photoelectron will increase by the same amount. If the electron emitted in the first step comes from an inner shell, there is now an inner shell vacancy (core hole) in the singly charged ion X^+. As was discussed in section 1.4.2, an Auger decay may follow, which 'fills' the core hole in state A and lowers the energy of the system to a new state, B, of the doubly charged ion X^{2+} (see figure 1.9). The Auger electron which is emitted in the secondary process will have a kinetic energy that equals the energy difference between the states A and B; $\varepsilon^{\mathrm{Aug}} = \varepsilon_A - \varepsilon_B$.

Aternatively, the system may go directly from the ground state of X to state B of X^{2+} by a double photoionization process. In this case, which is illustrated in the right panel of figure 1.9, the energy of the photon is used to remove two electrons simultaneously. The energy of the two photoelectrons is $\varepsilon_{\mathrm{tot}} = \varepsilon_1^{\mathrm{ph}} + \varepsilon_2^{\mathrm{ph}} = h\nu - \varepsilon_B$, and the two electrons can share the available energy arbitrarily.

These three different processes can be identified in the data sets by their different characteristics. Electrons from single photoionization and Auger electrons can be separated by varying the photon energy since the latter have fixed kinetic energies independent of photon energy, whereas the kinetic energy of the former varies as a function of photon energy. This method can also be used to distinguish direct double photoionization and double Auger decay in triple ionization data. The continuous energy sharing between the electrons in direct double photoionization is easy to recognize in a coincidence map such as the one shown in figure 1.10. It is important to remember that the spectrometer cannot separate between photoelectrons and Auger electrons. Instead, the electrons are sorted, and numbered, by their arrival time. Hence ε_2 is by def-

inition smaller than ε_1, which is apparent in the maps. The coincidence maps in figure 1.10 are plotted with the kinetic energy of the first and last electron on the x and y axes, respectively.

In the process depicted in the left panel of figure 1.9, the photoelectron and the Auger electron have fixed kinetic energies, in this example the Auger electron has a higher kinetic energy than the photoelectron ($\varepsilon_1^{\mathrm{Aug}} > \varepsilon_2^{\mathrm{ph}}$). Therefore, this two-step double ionization process gives rise to a well-defined spot in the map.

In the direct double photoionization process, the energy sharing between the two photoelectrons gives rise to a straight line in the coincidence map. We can confirm that the two electrons share a constant energy in the this process by plotting the summed energy along the y-axis as shown in figure 1.11.

Depending on which aspect one wants to visualize, different modes of visualization can be used. See for instance section VI (p. 116) in Ref. [14] for further discussion.

2. Multiple ionization of atoms and molecules

2.1 Background

Multi-ionized atoms and molecules have been studied using a large number of techniques during the hundred years (see e.g. Ref. [15] for a comprehensive review) and only a few will be mentioned here. Doubly charged atomic species were studied as early as in 1921 [16] by means of mass spectroscopy. Mass spectroscopy is insensitive to the electronic state of the ion, but has been used to determine ionization potentials [17], lifetimes of metastable doubly charged ions [18] and the kinetic energy release [19] in dissociation processes. Auger spectroscopy [20, 21] provides a wealth of information on the energy levels of, and transition pathways to multiply charged species. Several Auger mechanisms were described in section 1.4.2, and it is sufficient to mention here that the absence of strict selection rules and the great number of possible decay pathways often give rise to congested spectra (with overlapping lines).

Coincidence measurements of ions and/or electrons are given acronyms depending on the detected species such as PEPECO for photoelectron-photoelectron coincidences, PIPICO for photoion-photoion coincidences, PEPICO for photoelectron-photoion coincidences and so forth. The ionization process can be initiated in different ways, involving photons or charged particles, but photoionization has many advantages. Lablanquie *et al.* [22], were among the first to study double photoionization processes by electron-electron coincidence detection. In their experiment, an electrostatic electron analyzer was used in combination with a time-of-flight drift tube for low energy electrons. Later PEPECO studies utilized electrostatic analyzers [23] and magnetic bottle time-of-flight spectrometers [24, 25] developed by one of the pioneers in the field of coincidence spectroscopy, John Eland at Oxford. In success to the works of Refs. [22, 23, 24], the threshold photoelectron coincidence technique (TPEsCO) [26, 27], which detects electrons with almost zero kinetic energy, was developed. Although the TPEsCO technique has a very high energy resolution, it only provides information in the limited cases where at least one electron is emitted with zero kinetic energy. (Some variants of the technique also detects electrons with high kinetic energy, e.g. Auger electrons, in coincidence with a threshold electron.) The techniques discussed so far give limited information on the momenta of the charged particles. The COLd Target Recoil Ion Momentum Spectroscopy (COLTRIMS) [28, 29], as developed in

the group of Horst Schmidt-Böcking in Frankfurt, provides such information on the fragmentation processes with great detail. See e.g. Ref. [30] for a review on TPEsCO and COLTRIMS, and Ref. [31] for a more recent review on COLTRIMS.

The magnetic bottle time-of-flight coincidence technique introduced in 2003 [25], has proven to be a powerful tool for the study of double and higher order ionization processes, and it has the advantage of measuring electrons over a large kinetic energy range (0 to several hundred eV). Such a spectrometer is described in detail in section 3.3.1. Since its introduction, it has been used in many studies, see e.g. Ref. [14].

The adaptation of the magnetic bottle time-of-flight spectrometer to synchrotron radiation light sources, as demonstrated in the work of Penent *et al.* [32] has made it possible to study multi-ionization processes involving electrons from inner shells. See e.g. section VII B (p. 124) in Ref. [14] for a recent review. For example, core-valence double ionization of atoms and molecules [33] and Auger decays [34] have been studied. Also direct triple photoionization [35, 36] has been reported, as well as indirect ionization to higher ionization levels [34]. The fast repetition rates at synchrotron light sources are not ideally suited to such time-of-flight measurements, since the flight-times of the detected particles is often longer than the inter-pulse period of the ionizing light pulses. Several methods exist to overcome this problem, some of which are discussed further in section 3.3.2.

2.2 Single photon double ionization

Papers II–VI discuss experiments where two electrons are ejected simultaneously from the system upon absorption of a single photon. The single-photon double ionization process[1], DPI, is much less likely to occur than 'normal' single ionization and is difficult to model theoretically. See e.g. Ref. [38] for a review, and paper II for a more detailed discussion.

In this section, I will first discuss some general properties of double photoionization where two electrons are removed from the outermost valence orbitals, and then give some comments on DPI when one of the two electrons is removed from an inner (core) orbital.

2.2.1 Valence-valence ionization

We first consider double ionization from the valence orbitals of an atom. Removing an electron from any orbital requires a certain minimum amount of energy, referred to as the ionization energy (IE). In the resulting ion, the electrons are attracted by a stronger electric field than in the neutral atom, because

[1] The term photodouble ionization (PDI) is also used in the literature [37].

there are fewer electrons to 'screen' the nucleus. Hence more energy is required to remove a second electron than to remove the first. In the work of Tsai and Eland [39], an approximate ratio between the lowest ionization energies of

$$\frac{\varepsilon\{\text{Double ionization}\}}{\varepsilon\{\text{Single ionization}\}} = \frac{\varepsilon_{\text{DIE}}}{\varepsilon_{\text{IE}}} \approx 2.8 \tag{2.1}$$

was empirically determined.

Double ionization of molecules is more complex compared to atoms, since they may dissociate, or change their geometrical structure. Besides these two properties, also the localization of the holes in the molecule becomes important. In general, the electrostatic potential (Coulomb energy) between two particles with charges q_1 and q_2, i.e. the energy required to remove one of the charges, is simply

$$V = \frac{1}{4\pi\varepsilon_0\varepsilon_{\text{r}}}\frac{q_1 q_2}{r} \tag{2.2}$$

where r is the distance between the particles and $\varepsilon_0\varepsilon_{\text{r}}$ is the electric permittivity of the medium between them.

In the singly ionized molecule, we can think of the removed electron as a positively charged 'hole'. Taking the Coulomb energy required to remove a second electron explicitly into account, we can model the lowest double ionization energy as

$$\varepsilon_{\text{DIE}} = k \cdot \varepsilon_{\text{IE}} + \frac{g}{r_{\text{h–h}}} \tag{2.3}$$

where k and g are two constants to be determined experimentally and $r_{\text{h–h}}$ is the distance between the holes in the dication (the doubly charged ion), as discussed in the work of Molloy *et al.* [40]. Since the two holes have the same charge, they repel each other, and one may expect them to be as far away from each other as possible in the molecule. If there is a 'heavy' element in the molecule, it is likely that one hole is localized there. In hydrocarbon chains the (p-) orbitals hybridize and hence the hole is probably more delocalized in this case.

The single and double ionization energies were investigated for a large number of molecules by Molloy *et al.* [40], which led to the following empirical 'rule of thumb' for the lowest double ionization energy in molecular systems:

$$\varepsilon_{\text{DIE}} = 2.20 \cdot \varepsilon_{\text{IE}} + \frac{11.5}{r_{\text{h–h}}}, \tag{2.4}$$

where the energies are given in eV and $r_{\text{h–h}}$ in Ångström.

In paper III we present a study where we have tested the rule of thumb for a series of alcohol molecules which were not considered in Ref. [40]. The results are summarized in chapter 4, section 4.2.

2.2.2 Core-valence ionization

Core-valence double photoionization spectra of molecules have some features that cannot be observed in valence-valence double ionization. To a first approximation, one may expect the core-valence photoelectron spectrum to resemble the ordinary valence photoelectron spectrum, but shifted by the extra energy needed to remove an electron from the inner shell plus the coulomb interaction of the two vacancies. Some of the core-valece double ionization spectra presented in section 4.3 show that this model actually works quite well. However, the spin-spin interaction of the holes needs to be considered. Closed shell molecules like CS_2, SO_2 and OCS have zero spin in the neutral ground state, and hence the dicationic species form singlet and triplet states (if *LS*-coupling is valid). O_2 has two unpaired electrons in the neutral ground state, yielding a total spin of 1 (a triplet). Therefore singlet, triplet and quintet states can be formed in core-valence ionized O_2.

Two obvious properties that can be studied when comparing valence photoelectron spectra and core-valence spectra are thus the shift of corresponding line structures, and possibly splittings due to spin-spin interaction. According to an article by Schulte, Cederbaum and Tarantelli [41] these two properties can be directly related to the distance between the holes, which also tells us something about the localization of the holes. Core-valence double ionization have been studied in a few molecules by Hikosaka *et al.* [33, 42].

It may not, however, be trivial to determine the shifts and splittings from complex experimental spectra. To facilitate the interpretation of spectra it is useful to calculate the energy levels. Such calculations of core-valence levels presented in this thesis have been carried out using a multi-configuration self consistent field (MCSCF) approach, in collaboration with theoretical research groups. Since we are interested in processes involving both inner shells and valence electrons, the calculation easily grows to an unmanageable size. This can be overcome by dividing the orbitals into different sets and then do the calculations on each set separately (see Ref. [43] for a more detailed description).

3. Experimental techniques

In the coincidence measurements presented in this thesis, we have measured the kinetic energy of several electrons, sometimes in coincidence with the resulting ions. The kinetic energy of each electron is determined by measuring the time it needs to travel a fixed distance, and this technique requires short (a few ns) light pulses and sophisticated timing schemes. It is also necessary that the light pulses are intense, and have well defined photon energies. We study gaseous samples, and the experiments must be performed in vacuum since both the soft x-ray photons and the emitted electrons are otherwise easily absorbed.

This chapter first gives a brief introduction to coincidence spectroscopy and then presents two light sources we have used: a pulsed helium discharge lamp and synchrotron radiation produced by an undulator. The magnetic bottle electron time-of-flight spectrometer is presented and some timing schemes for determining the flight-times of the ejected electrons are discussed. Finally a setup for detecting ions as well as electrons is presented.

3.1 Coincidence spectroscopy

The purpose of any coincidence experiment is to selectively study two or more particles originating from a single primary event. In the experiments presented in this thesis, this translates into the simultaneous detection of all the electrons ejected as a result of the absorption of a single photon. In some of the experiments presented in paper VI we have also detected the resulting ions in coincidence with the electrons. The flight times of the electrons (and ions) are registered using a common-start-multi-stop timing scheme, and particles that hit the detector within a certain time window are considered to be part of the same coincidence event. There are, however, also uncorrelated particles which hit the detector in a random way, and some of these will accidentally be registered as coincidence events. The background signal from such false coincidence events must be kept as low as possible, since the signal from the true coincidence events is often rather weak.

3.1.1 Coincidence statistics

As mentioned in section 2.1, there are many different setups for measuring electron-electron or electron-ion coincidences, and they are described by slightly different statistical models. In the present electron-electron setup, all the electrons are detected using a single detector, and the apparatus has an approximately constant collection-detection efficiency of about 50%. In all the measurements presented in this thesis, electrons with kinetic energies ranging from zero to several hundred electron volts are measured simultaneously, i.e. with full multiplex. It should also be noted that we measure *multi*-coincidence *events*, and consequently the accidental detection of a false *hit* does not prevent the detection of true ones. There is, however, a short dead-time ($\sim$ 10–50 ns) in the detector, which prevents the measurements of two electrons of the same or very similar kinetic energies. Detection of false coincidences may cause problems, since for instance a two-electron event detected in coincidence with a random electron is registered as a 3-electron event, and conversely, a 3-electron event where the equipment fails to detect one of the electrons is registered as a 2-electron event. In the case of core-valence double ionization, the two photoelectrons are often detected in coincidence with an electron from the subsequent Auger decay. This is actually a useful feature, since the background is generally lower in 3-electron data (all coincidence events where exactly three electrons have been detected) than in 2-electron data. Furthermore, the 3-electron data can be filtered by rejecting all events where the Auger electron (which has a known kinetic energy) is not present.

The part of the background which is caused by accidental registration of unrelated hits within the time window of a coincidence event can be described by a Poisson distribution. The probability of detecting exactly *n hits* (occurrences) during the time window τ of a coincidence event is

$$P(n) = \frac{\lambda^n}{n!} e^{-\lambda}, \tag{3.1}$$

where λ is the average number of hits per coincidence event. It should be noted that the background depends strongly on the kinetic energy of the electrons and a high rate of false events is perfectly acceptable if the corresponding structures in the coincidences map don't interfere with the structures caused by the true coincidences. For instance, the background in a two-electron data set is generally enhanced at energies where the cross section of single ionization is large, and the true events can be separated from such false events by a careful choice of photon energy.

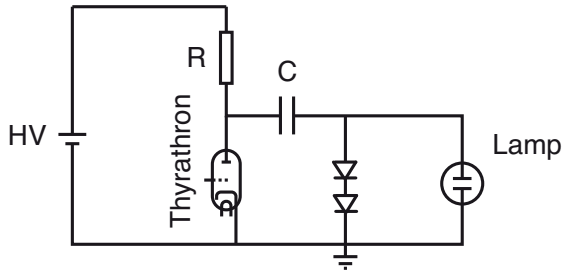

Figure 3.1: Electronic schematic of the pulsed helium lamp used in our laboratory [44].

3.2 Light sources

Time-of-flight measurements of electrons ejected in multi-ionization processes put certain demands on the light source which creates the ionizing light pulses. Firstly, the photons need to be sufficiently energetic to cause the release of the relevant electrons, and secondly, the light pulses need to be short compared to the flight-times of the electrons. Moreover, the cross section of single photon double photoionization, which is one of the main themes of this thesis, is comparatively small. Therefore, an intense pulsed light source which emits photons in the relevant spectral region is required.

3.2.1 A pulsed He lamp

In our laboratory in Stockholm we have used a pulsed hollow cathode discharge lamp [46], originally developed by John Eland at Oxford (see e.g. Refs. [25, 44]), as light source. The lamp generates discharges in a capillary filled with helium gas, which flows through the lamp. These discharges create light of several discrete energies in the vacuum ultraviolet range, which

Table 3.1: *Main lines present in the radiation of the He lamp used in our laboratory [45].*

Atomic line	Electronic transition	Wavelength (Å)	Energy (eV)
He Iα	$1s2s\,^1P_1 \rightarrow 1s^2\,^1S_0$	584.33	21.22
He I	$2p^2\,^3P \rightarrow 1s2p\,^3P$	320.29	38.71
He IIα	$2p\,^2P \rightarrow 1s\,^2S$	303.78	40.81
He IIβ	$3p\,^2P \rightarrow 1s\,^2S$	256.32	48.37
He IIγ	$4p\,^2P \rightarrow 1s\,^2S$	243.03	51.02

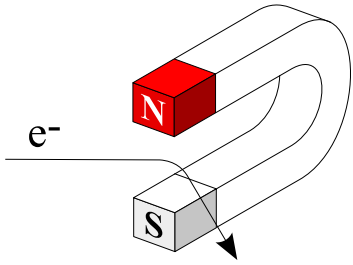

Figure 3.2: The trajectory of an electron is bent in a magnetic field.

are listed in table 3.1. We have mainly used the HeIIα and HeIIβ lines for valence-valence double photoionization studies.

A circuit diagram of the He-lamp is shown in figure 3.1. Since we need very short light pulses ($\sim$ 5–10 ns), the discharge must be very fast. It is generated by first charging a capacitor connected to the hollow cathode in the lamp and then using a fast hydrogen thyratron to rapidly set the potential on the voltage supply side of the capacitor to zero, thereby creating a short-circuit to ground. The charge on the cathode side of the capacitor must then go through the helium gas, creating a discharge between the cathode and the anode. Quenching of the discharge keeps the light pulse short and the whole process is repeated a few thousand times per second. The light is then focused onto the sample by a toroidal grating monochromator, which is used to select the desired He emission line.

3.2.2 Synchrotrons

Another way of generating ionizing electromagnetic radiation is to take advantage of a phenomenon known as synchrotron radiation, which is the result of several physical effects. One important effect is that magnetic fields bend the trajectories of charged particles (see figure 3.2), and another effect is that charged particles emit electromagnetic radiation when they are accelerated.[1] It is thus possible to generate electromagnetic radiation by accelerating charged particles using magnetic fields. However, as mentioned before, we need a pulsed source which emits many photons in the VUV and soft x-ray spectral regions. This can be achieved by accelerating electrons to highly relativistic speeds, i.e. nearly the speed of light. At these speeds, the emitted radiation is highly energetic and directed in a narrow cone tangent to the path of the electron. To do this requires a lot of energy, and moreover, the electrons lose energy when they emit synchrotron radiation. It is also necessary to control the trajectories of the electrons in a precise manner. The technique may

[1]The second phenomenon is put to use in antennas where the transmitting antenna converts an electrical signal (moving charges) to radio waves and the receiving antenna recovers the signal by the inverse process.

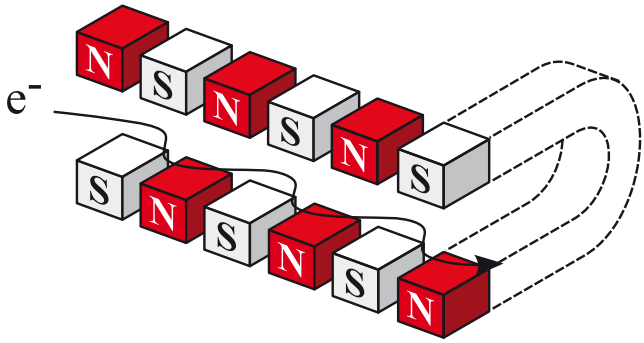

Figure 3.3: Schematic picture of the path of an electron bunch in an undulator.

seem quite complex, but synchrotron light is generated on a routine basis in approximately 50 synchrotrons around the world [47]. In a synchrotron, electrons are grouped in bunches which are circulated in a storage ring. Every time an electron bunch's trajectory is bent by a magnetic field it emits electromagnetic radiation and, to take full advantage of this effect, dedicated 'insertion devices' are used. One such device, which has been used in the synchrotron based experiments presented in this thesis, is the so-called undulator.

3.2.2.1 Undulators

The basic design principle of the undulator is to arrange magnets with alternating north and south poles as shown schematically in figure 3.3. When an electron bunch passes through the undulator, the bunch 'wiggles' left and right due to the alternating magnetic fields. The many fast turns produce high intensity electromagnetic radiation, emitted in the forward direction of the electron bunch. Because of the combined effect of the length contraction of the undulator and the relativistic Doppler shift of the wavelength when performing Lorentz transformations between the frames of reference of the electron bunch of the laboratory, the emitted electromagnetic radiation lies in the soft x-ray spectral region. In analogy with the He discharge lamp used as light source in our home laboratory, one needs to select light of the desired wavelength and focus the beam onto the sample. A feature of the undulator is that the wavelengths of the emitted light can be controlled by changing the distance between the two magnet arrays. The possibility to 'tune' the wavelength makes undulators versatile for a wide range of experiments. A more thorough description of synchrotron radiation and undulators can be found in Ref. [48].

3.2.2.2 Time structure of a storage ring

One or several electron bunches can be stored simultaneously in the synchrotron storage ring. The first mode of operation is referred to as single-bunch and the latter one is called multi-bunch mode. Since it is necessary to identify

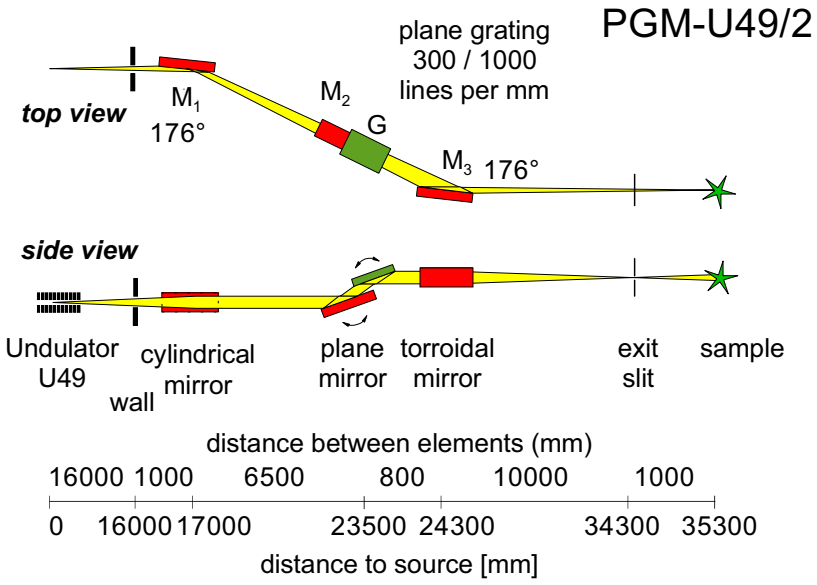

Figure 3.4: The U49/2 PGM 2 beamline at BESSY II. Credit Ref. [50]

the ionizing light pulse to be able to measure the time-of-flight of the detected electrons (or ions), it is indispensable to have a sufficiently long inter-pulse period between light pulses, which is directly related to how often an electron bunch passes through the insertion device. The synchrotron based experiments presented in chapter 4 have been carried out at the BESSY II storage ring [49] during single bunch operation. This mode of operation is advantageous for our experiments, since it has a longer time period between light pulses. At BESSY II, the time period in single bunch mode is 800.5 ns and the width of the light pulses is approximately 30 ps [49]. We will come back to the time structure when timing schemes for time-of-flight measurements are discussed in section 3.3.2.

3.2.2.3 Beamlines

The beamline conveys the light from the insertion device to the experimental setup. Often several setups are connected to the same insertion device, and the beamlines branch out to the different setups. There are many different beamline designs, some aiming for high energy resolution, while at the same time keeping as much of the intensity as possible. The energy range is selected using a monochromator (see next section) and the light beam is focused by using mirrors to image the source onto the sample. Since light intensity is lost in every optical reflection (to a lesser degree if the incident angle is small, i.e. grazing), one usually seeks to use as few reflections as possible. See e.g. Ref. [51] for more details on beamline design.

The synchrotron based experiments presented in this thesis were performed at the beamlines U49/2 PGM-1 [52, 53] and PGM-2 [54] at the BESSY-II [49] storage ring in Berlin. Both beamlines are connected to the same undulator (U49/2) and provide light in the soft x-ray energy region ($\sim$ 86–1600 eV), which covers several of the inner shell ionization energies of the systems we have studied. The optical layout of beamline PGM-2 is shown in figure 3.4 and beamline PGM-1 has a similar optical layout. A significant difference is that beamline PGM-1 is equipped with a refocusing mirror after the monochromator. In our experiment, a wide spot will broaden the time-of-flight distributions, but the nominal spot size of beamline PGM 2 of approximately 500 μm in the plane of the flight tube (the horizontal plane) is sufficiently small without further focusing for most of the experiments performed. In the electron-ion coincidence experiment presented in paper VI a smaller focus ($\sim$ 280 μm) was necessary for unambiguous identification of the lines in the mass spectrum. This was achieved by moving baffles into the light path. The size of the spot in the perpendicular plane (vertical), which depends on the size of the exit slit of the monochromator, affects the resolution of the magnetic bottle spectrometer less.

3.2.3 Monochromators

The light sources we have discussed produce electromagnetic radiation of several wavelengths, but for the experiments presented here, it is important to use a well-defined wavelength for the excitation process. In the soft x-ray spectral region, the most common method of separating radiation of different wavelengths is to use a diffraction grating. This device consists of a precise pattern of microscopic periodic structures which diffract the light. Usually this pattern is a grid of reflecting lines made out of a corrugated surface coated with a metal to enhance reflectivity. According to the Huygens–Fresnel principle, the reflecting lines can be considered as thin coherent light sources emitting light in all directions. If we let θ_{in} and θ_{out} denote the angles of incidence and reflection of the light beam relative to the normal, it can be shown that for a grating with a periodic distance between the reflecting lines of d, constructive interference from the thin local emitters is obtained when

$$d(\sin(\theta_{\text{in}}) - \sin(\theta_{\text{out}})) = n\lambda, \quad n = 0, \pm 1, \pm 2, \ldots \tag{3.2}$$

where λ is the wavelength of the light and n is the order of diffraction. Hence the grating separates light of different wavelength into different reflection angles (except in the zeroth order which is simply normal reflection). For further reading, see e.g. Ref. [55].

As mentioned above, a compact monochromator consisting of a toroidal grating which also acts as a focusing mirror has been used for the He lamp based experiments. The monochromators used at synchrotron radiation facili-

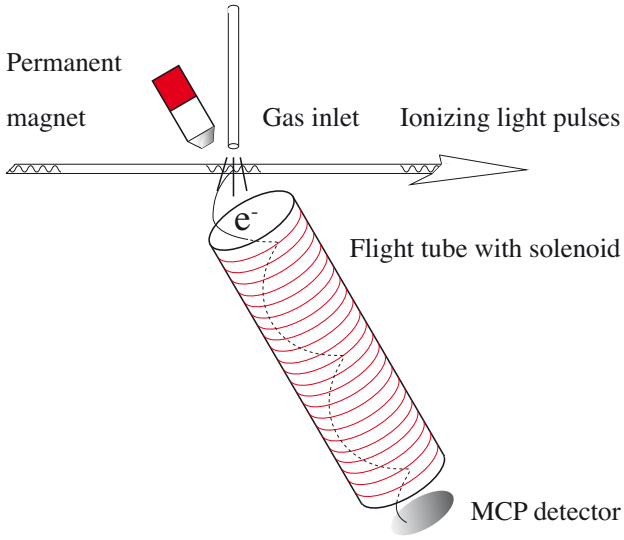

Figure 3.5: Overview of the magnetic bottle time-of-flight setup.

ties are often considerably larger instruments. These monochromators need to provide stable operation over a large energy range despite the heat load from the synchrotron. The monochromators used at beamlines U49/2 PGM 1 and 2 have similar characteristics although the most highly resolving grating of the PGM 1 monochromator has 1200 lines/mm compared to 1000 lines/mm for the PGM 2 monochromator. During many of the experiments presented in this thesis, we have limited the ionization rates in order to keep the number of false coincidence events low. This was achieved by using very narrow monochromator exit slits (see figure 3.4), which reduces the flux of the ionizing radiation. As a consequence, the energy bandwidth of the ionizing soft x-ray radiation becomes narrow and has hence not been a limiting factor in these experiments.

3.3 Experimental setup

3.3.1 The magnetic bottle time-of-flight-spectrometer

The basic idea behind a time-of-flight electron spectrometer is to determine the kinetic energy of an electron by measuring its speed. This is achieved by placing a detector at a known distance and measuring the travel time of the electron between the locations where it is emitted and detected. Since the electrons are easily absorbed by air it is necessary to perform the experiments in a 'flight tube', which is kept under vacuum. In the magnetic bottle spectrometer [25, 56], the electrons are guided to the detector by a weak magnetic

field generated by a solenoid wound around the flight tube. The sample gas is photoionized in the interaction region, where the magnetic field lines of the solenoid are contracted by a permanent magnet. The resulting magnetic field acts as a magnetic mirror, which reflects the electrons into the flight tube (cf. figure 3.5). Together with the solenoid, the permanent magnet forms a 'magnetic bottle', which efficiently collects the electrons and guides them to the detector without changing their kinetic energies. (The Lorentz force is always perpendicular to the electron motion and hence zero work is done by the magnetic field. Furthermore, the speed of the electrons is much lower than in an synchrotron, and they do not lose significant amounts of kinetic energy by emitting electromagnetic radiation.)

Because the processes we want to study usually have a small cross section, we can not afford to lose electrons, but we need to collect the electrons emitted in all directions, regardless of their kinetic energies. It is therefore important to tune the relative strength of the magnetic fields and to make sure that the ejected electrons are imaged onto the detector. The permanent magnet is mounted on a *xyz* motion stage which enables us to make adjustments without breaking the vacuum. In order to collect electrons with very low kinetic energies, a small electric voltages can be applied over the interaction region.

Figure 3.5 shows a schematic illustration of the magnetic bottle time-of-flight spectrometer. The sample gas is let into the ionizing chamber through a needle, and the light hits the effusive gas jet perpendicularly, which defines a small ionization region in the centre of the ionization chamber. The pressure of the gas can be controlled by a fine-adjustable needle valve and the temperature of the gas in the plane perpendicular to the neddle can be varied by changing the distance between the needle and the light beam. The entire setup is kept under vacuum to avoid absorption of the emitted electrons or the ionizing radiation anywhere except in the interaction region.

After the ionization event, the emitted electrons are caught by the magnetic field of the permanent magnet and the solenoid, and guided toward the detector at the far end of the 2.2 metres long flight tube by the solenoid field. A μ-metal shield (not shown in figure 3.5) protects the electrons from external magnetic fields.

The electrons are detected using a micro-channel plate (MCP) detector which basically amplifies the charge of the electron. A MCP plate consists of a thin glass wafer perforated by a large number of small holes or channels (~ 0.01 mm in diameter). Each time an electron hits the inner wall of a channel, a small shower of secondary electrons is released. Several MCP plates are put together in a stack, and by applying a high voltage across the stack, the electrons are accelerated toward an anode. Since new electrons are released every time an electron hits the wall of a channel, there is an 'avalanche effect' (similar to the mechanism of a photomultiplier tube) and one electron can result in a $\sim 10\,000$-electron swarm hitting the anode.

The signal from the anode is connected to the timing electronics where it is referenced to a 'start pulse' from the light source. The time difference between the signal from the anode and the signal from the light source, i.e. the time-of-flight of the electron, is registered by a time-to-digital converter and stored in a computer.

This magnetic bottle spectrometer design makes it possible to detect kinetic energies ranging from zero to hundreds of eVs. The energy resolution of single electrons is about 20 meV at kinetic energies below 1 eV and at higher kinetic energies the numerical resolution can be expressed as $E/\Delta E \sim 50$.

3.3.2 Timing

In our coincidence experiments, all the electrons which are detected within a certain time window are associated with a specific ionization event, created by a specific ionizing light pulse. Since we usually want to study 'weak' processes, it is important to measure at count rates that are sufficiently low to avoid 'false' coincidence events. If the count rate is too high, we risk accidental detection of electrons from separate ionization events during the time window of a coincidence event. It is equally important to detect as many of the emitted electrons as possible.

The most straightforward way of measuring the flight-time of an electron is to use the ionizing light pulse itself (the reference signal from the light source can be obtained in several ways) to start the time measurement and then register the arrival times of the electrons at the detector. If no ionization event took place one simply stops measuring after some time, typically $\tau \sim$ 5–10 microseconds in a 2 metres instrument. As long as the light source pulses arrive with longer intervals than τ, there is no risk of mixing up electrons created by two different pulses. The He lamp used in our laboratory in Stockholm works at repetition rates of a few kilohertz, which is well suited for the described timing scheme.

Synchrotron light sources, however, work at considerably higher repetition rates, typically a several hundred MHz. Even when operated in single bunch mode, i.e. with only one electron bunch in the storage ring, the inter-pulse period at the BESSY II facility, where we have performed the sychrotron radiation based experiments presented in this thesis, is 800.5 ns [49]. Consequently, there is a risk of referencing the flight-times of the electrons to another light pulse than the one causing the ionization event if the flight-time exceeds 800 ns (compared to ~ 5 μs in the case of the He lamp). A flight-time of 800 ns corresponds to a kinetic energy of approximately 20 eV, which is an obstacle for some measurements.[2] However, it is sufficient if one knows that the most

[2]Since one can estimate the maximum possible kinetic energy of any electron (e.g. not more than the photon energy used) one can add a time period (i.e. 800 ns) to flight-times that are obviously to low. This pushes the minimum kinetic energy down from 20 eV to approximately 10 eV.

energetic electron created in an ionization event arrives at the detector within the time period of the light source, i.e. 800.5 ns at BESSY II [49]. It is then possible to identify the light pulse which caused the emission of the first, most energetic, electron, and electrons created in the same ionization event arriving later can be referenced to the same light pulse [32]. One can hence use the fast electron as a start signal and wait e.g. 5 μs to collect also the slow, less energetic, electrons with low risk of confusing electrons from different ionization events. It is therefore viable to use the magnetic bottle time-of-flight coincidence technique at synchrotron light sources provided that at least one of the electrons has a sufficiently high kinetic energy. Alternatively, one can make use of a mechanical chopper [36, 57], which reduces the repetition rate of the light pulses. A third method, which was very recently demonstrated by our group [35], is to detect ions in coincidence with the electrons and use the flight-times of the ions to identify the ionizing light pulse. In fact, all three methods were employed in some of the experiments presented in this thesis. However, many ionization processes involve Auger electrons of sufficiently high kinetic energy ($>$ 20 eV), and the method described above is therefore well suited to study multi-ionization processes which involve such Auger transitions.

3.3.3 Time to energy conversion

The kinetic energy of the electrons are calculated in software from their flight-times, t. Assuming a straight path between the interaction region and the detector, and denoting the distance between them by l, we have

$$\frac{mv^2}{2} = \varepsilon^{\text{kin}} \text{ and } l = v \cdot t \implies \varepsilon^{\text{kin}} = \frac{ml^2}{2t^2} \tag{3.3}$$

where m denotes the mass of the electron and v its velocity. However, we need to take the time delay between the occurrence of an event and its registration into account, and, in addition, we need to compensate for electrostatic fields in the interaction region. Adding two calibration parameters t_0 and ε_0 to the previous equation gives the following simple relation

$$\varepsilon^{\text{kin}} = \frac{D^2}{(t - t_0)^2} + \varepsilon_0. \tag{3.4}$$

The constant D contains the length of the flight tube and the mass of the electron, but in practice its value is determined during the calibration of t_0 and ε_0.

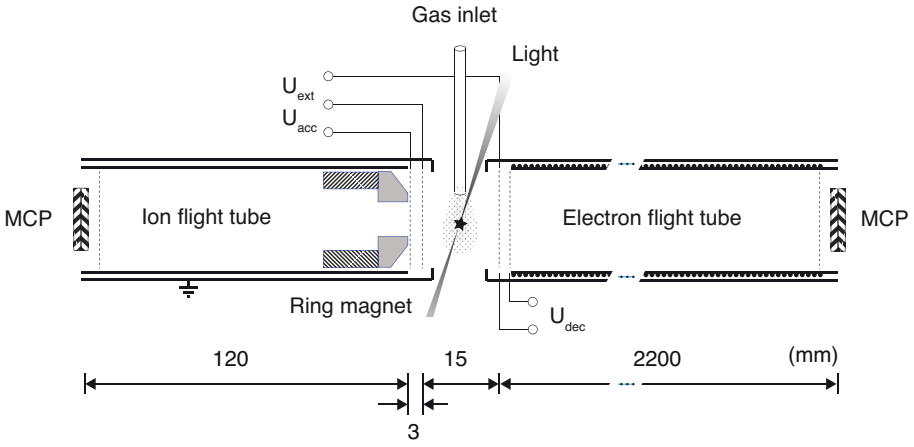

Figure 3.6: The electron-ion coincidence setup (cf. Refs. [58, 59]). U_{ext}, U_{acc} and U_{dec} denote voltages used to extract and accelerate ions and to decelerate electrons.

3.3.4 The ion time-of-flight setup

The time-of-flight technique can also be applied to ions. The main differences are that ions are heavier than electrons (and hence move more slowly) and that they can have several charge states. In paper VI we have used a short ion time-of-flight spectrometer [58, 59], which works as a two-field Wiley-Maclarin [60] mass spectrometer, to detect ions in coincidence with the electrons. The resolution in the measurement of the kinetic energies of the electrons is reduced in this setup, because the conically shaped permanent magnet of the original setup has been replaced by a ring magnet embedded in the ion mass spectrometer.

Detection of ions and electrons in coincidence allows us to associate electrons to different ionization stages more easily. Furthermore it makes it possible to use known ion flight times for identification of the ionizing light pulse. Figure 3.6 shows the electron-ion coincidence setup. The front end of the mass spectrometer consists of a ring magnet and a pierced conical soft iron pole piece, which replaces the conically shaped permanent magnet in the electron-only setup and creates the strong magnetic field. The ions are collected by applying an electric field between two grids situated on each side of the interaction region (see figure 3.6). Several modes of operation are possible and will be presented in the following section.

When the ions have entered the mass spectrometer they are first accelerated by a stronger field ($U_{\text{acc}} \sim 1000$ V). After passing through the hollow ring magnet, they enter a field free region which separates ions with different charge/mass ratio. The mass spectrometer is covered by a copper shield to prevent electric fields from 'leaking out' and affect the electrons.

Timing schemes for the ion time-of-flight setup

The most straightforward way of extracting electrons and ions in opposite directions using the setup described above is simply to wait a certain time until the electrons have left the interaction region and then apply an electric field to extract the ions (see e.g. Refs. [58, 59]). The latter are much heavier and stay in the interaction region much longer. The electron spectra are relatively unaffected by the the extraction field, since the electrons have already left the interaction region when it is applied. This approach has been used successfully with the He-lamp, but the fast repetition rate at synchrotron sources makes it impossible to wait for the electrons to leave the interaction region before applying the extraction voltage. Instead a small DC voltage (~ 7 V/cm) across the interaction region can be used to draw out the ions from the interaction region. The electrons are of course pushed in the opposite direction by the DC voltage, but a retarding field can be used to decelerate them before they enter the electron flight tube. This procedure serves to restore the energy resolution of the electrons. Appropriate tuning of the extraction and acceleration voltages makes it possible to separate different ions with different mass/charge ratios modulo the ring period (see e.g. Ref. [35] and paper VI). One can then identify electrons from specific atomic or parent molecular charge states. This identification makes it possible to unambiguously identify the ionizing light pulse even if all the electrons have kinetic energies below 20 eV. Detection of ions and electrons in coincidence also suppresses false coincidences in the spectra.

4. Summary of papers

4.1 Papers I and II: Creation of triply charged krypton via several ionization pathways

In papers I and II we present results on triple ionization of Kr involving the creation of a 3d hole. Besides the removal of a 3d electron, one can also expect the initial ionization process to produce shake-up states [61] and double photoionization to $3d^{-1}4p^{-1}$ core-valence ionized Kr^{2+} [62]. Figure 4.1 shows a coincidence map of triple ionization of krypton recorded at $h\nu = 150$ eV. The x-axis represents the total kinetic energy of all three electrons emitted, and the y-axis represents the kinetic energy sum of the two slower electrons. Dark pixels in the coincidence map signify larger intensity and the grey scale is chosen to enhance weak features. The different spots and lines correspond to different processes, some of which are illustrated in the energy diagram in figure 4.2. There are apparently several different ionization pathways contributing to the triple ionization data set, and a great strength of the coincidence technique is the possibility to discriminate between them. Indeed, three distinct groups of features are revealed in figure 4.1, corresponding to the three different initial hole states. Starting from the top of the figure, we attribute these features to: a) double Auger decay from initial $3d^{-1}4p^{-1}nl$ states, b) normal Auger decay from $3d^{-1}4p^{-1}$ core-valence ionized states of Kr^{2+}, and c) double Auger decay from initial $3d^{-1}$ states.

4.1.1 Experimental details

Krypton triple ionization electron coincidence data were recorded at beamline U49/2 PGM 2 (see section 3.2.2.3 and Ref. [54]) at the BESSY-II storage ring in Berlin using 140 and 150 eV photons. Depending on the ionization pathway, the first arrival electron, which is used as the start signal of the coincidence measurement, was either a photoelectron or an Auger electron. In both cases the flight times of the electrons were related to the ionizing light pulse by using the ring clock as time reference. The spectrometer was configured for electron detection as described in section 3.3.1.

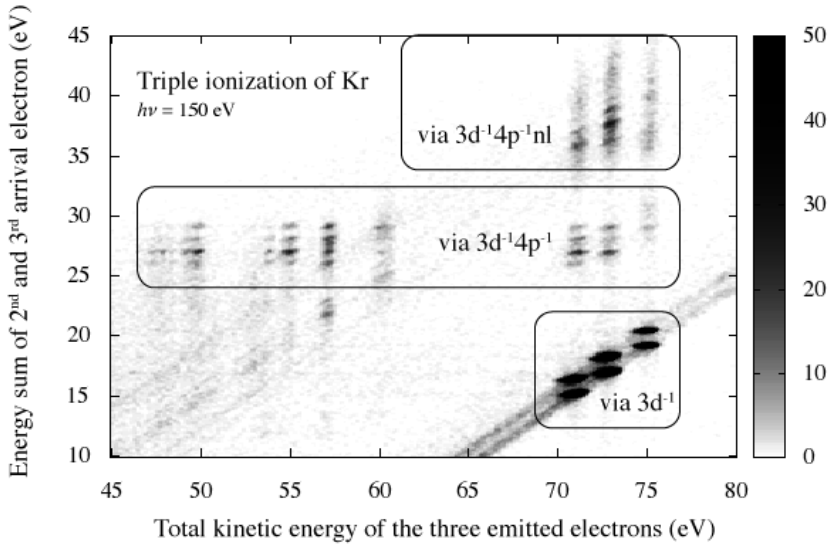

Figure 4.1: Coincidence map of triple ionization of krypton recorded at a photon energy of $h\nu$= 150 eV.

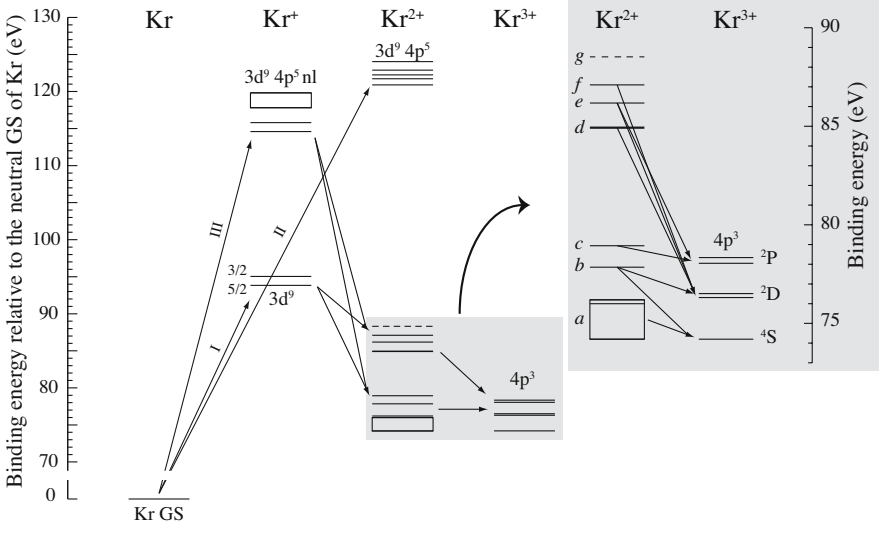

Figure 4.2: Kr triple ionization pathways involving an initial 3d hole.

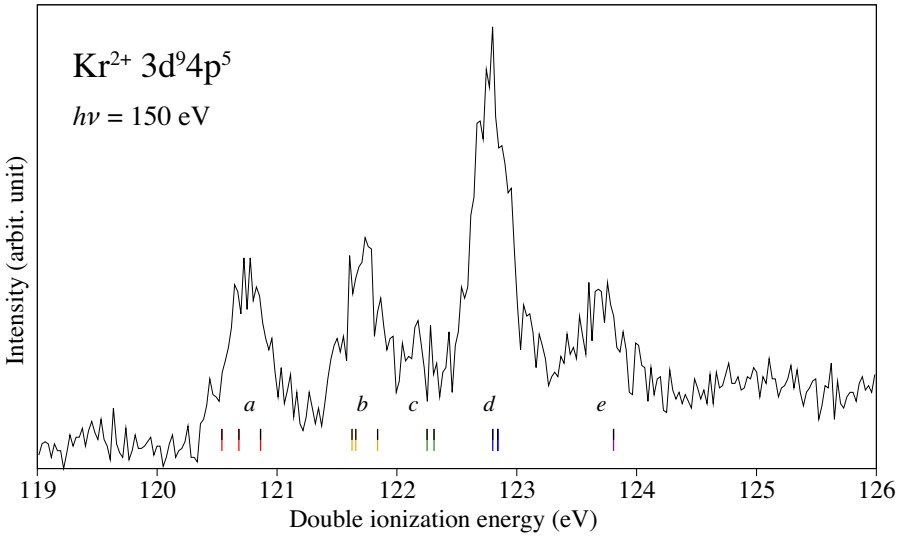

Figure 4.3: Core-valence double ionization electron spectrum of Kr^{2+} recorded at a photon energy of 150 eV.

4.1.2 Results and discussion

The spectrum reflecting core-valence double ionization to the $3d^{-1}4p^{-1}$ states of Kr^{2+} is shown in figure 4.3. This spectrum is obtained by projecting the middle group of coincidence events in figure 4.1 onto the vertical axis. The spectrum shown in figure 4.3 agrees well with the TPEsCO spectrum of Bolognesi *et al.* (figure 1 in Ref. [62]), which is interesting since the spectrum of Ref. [62] was recorded at threshold, while the spectrum presented in figure 4.3 was recorded about 30 eV above threshold. Several calculations of corresponding energy levels are available in the literature (see e.g. Refs. [62, 63, 64, 65]), which differ mainly in the *LS* assignments. New calculations using the multiconfiguration Dirac-Fock (MCDF) method [66] have been carried out by a collaborating research group The calculated energies are plotted as vertical bars in figure 4.3 and agree well with those presented in Ref. [62].

The $3d^{-1}4p^{-1}$ states are likely to decay to Kr^{3+} by emission of an Auger electron. Since the photoelectrons and Auger electrons are detected in coincidence, it is possible to selectively study the Auger electrons from states belonging to each peak structure in figure 4.3. The resulting spectra are presented in paper II, but the main trends can readily be observed in figure 4.1. In particular, two noteworthy features are visible in the part labelled $3d^{-1}4p^{-1}$. The final tricationic states corresponding to kinetic energy sums of 60 and 75 eV (x-axis) are populated mainly from intermediate state corresponding to the single spectral line with $\varepsilon_2 + \varepsilon_3 = 29$ eV (y-axis). The calculated energies of

Table 4.1: *Observed intermediate Kr^{2+} states in cascade double Auger decays from $3d^{-1}$ states of Kr^{+} to $4p^{-3}$ states of Kr^{3+}.*

Inter-mediate	Observed energy relative to Kr^{3+} ^4S (eV)	Final states of $4p^{-3}$ Kr^{3+} Dominant	Weak	Comment
a	0–2.0	^4S		Rydberg states
b	3.65	^2D	^4S	
c	4.80	^2P	^4S, ^2D	
d	10.9	^2D	^4S, ^2P	
e	12.0	^2D, ^2P	^4S	
f	12.9	^2D	^4S, ^2P	
g	14.5	(^4S), ^2D, ^2P		Low intensity

these intermediate states are shown below the line labelled *a* in figure 4.3. The final states can be identified as $4s^1 4p^4\ ^4P$ (60 eV) and $4s^2 4p^3\ ^4S$ (75 eV) as discussed in paper II. Calculations of the corresponding Auger rates, presented in paper II, display a similar selectivity it the population of these states.

The group of spots in the lower right corner of figure 4.1 corresponds to Kr^{3+} $4p^{-3}$ final states created by cascade Auger decays from an initial 3d hole state. These Auger cascades give rise to the dark spots in the coincidence map in figure 4.4. In the latter figure, the *y*-axis corresponds to the sum of the kinetic energies of the two Auger electrons. The projection onto this axis, which is presented in the left panel of figure 4.4, shows 6 peak structures since there are two initial states (the $D_{3/2}$ and $D_{5/2}$ components of the $3d^{-1}$ configuration of Kr^{+}) decaying to three final $4p^{-3}$ states of Kr^{3+} (^4S, ^2D and ^2P). The *x*-axis corresponds to the kinetic energy of the slower of the two Auger electrons. The various spots in the coincidence map can be associated with Kr^{2+} intermediate states, which are drawn schematically in fig 4.2. Their relative energies are listed in table 4.1. We find that there is a state (*c* in figure 4.2, labels 7 and 8 in figure 4.4), which decays almost exclusively to the $4p^{-3}$ ^2P final states of Kr^{3+}. We also find that the ^4S final state is populated from a sequence of intermediate states (label *a* in figure 4.2 and labels 1 and 2 in figure 4.4) that can be associated with Rydberg series converging onto $4p^{-3}$ ^2D and a state at higher ionization energy (*b* in figure 4.2, labels 3 and 4 in figure 4.4).

The topmost group of features in figure 4.1 corresponds to decays from $3d^{-1}4p^{-1}nl$ singly ionized states. Here the double Auger decays to Kr^{3+} ^4S states are dominated by decays via states in the Rydberg series labeled *a* in figure 4.2 (cf. paper I).

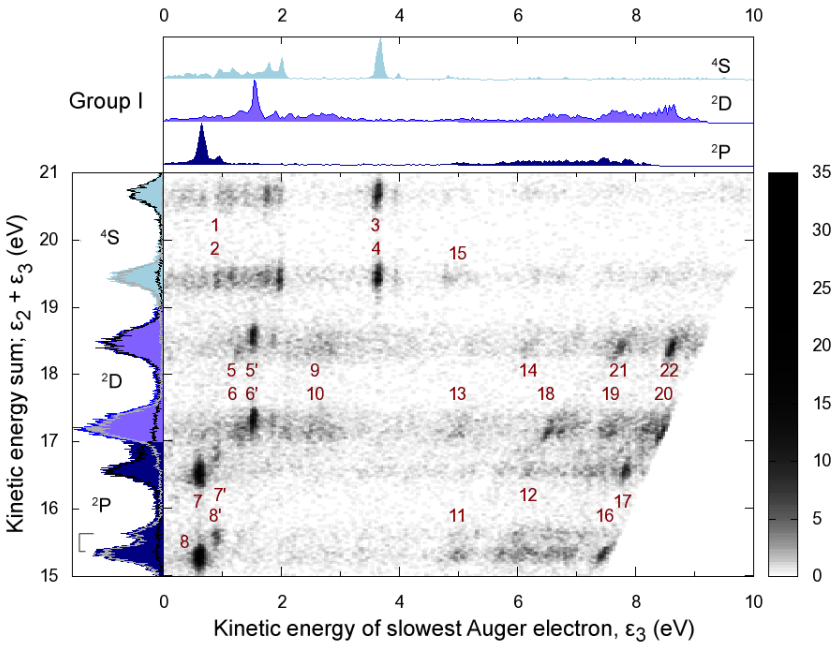

Figure 4.4: Coincidence map of triple ionization of Kr selected on 3d photoelectrons as the first arrival electron. The six stripes in the map corresponds to six possible combinations of the two initial 3d hole states and three resolved Kr^{3+} $4p^{-3}$ final states (^{4}S, ^{2}D and ^{2}P). The dark spots correspond to cascade Auger transitions. For further details, see text and paper I of this thesis.

Triple ionization of krypton using a photon energy of 91.2 eV, which is below the 3d threshold, was reported in Ref. [35], and these Rydberg intermediates seem to play a role also here.

4.2 Paper III: Double photoionization of alcohol molecules

In this experiment, we have studied the valence-valence double photoionization of three alcohols of increasing molecular size. The molecular structure of the three systems (methanol, ethanol, and n-propyl alcohol[1]) are shown in figure 4.5.

The valence-valence double ionization spectra were measured using the same magnetic bottle spectrometer as in the experiments presented in the pre-

[1]This substance have many names. The IUPAC name is Propan-1-ol [67].

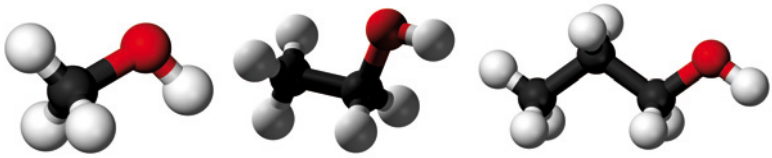

(a) Methanol *(b)* Ethanol *(c)* n-propyl alcohol

Figure 4.5: Molecular structures of the alcohol molecules in the neutral form. The colours used (in the digital version) are black for carbon, white for hydrogen and red for oxygen.

vious section, but using the pulsed He-lamp from the original Oxford setup[2] as light source. The He-lamp was discussed in section 3.2.1. A photon energy of 40.814 eV was used to ionize the vapours of the alcohols. The single ionization spectra were measured in Uppsala using a conventional electron spectrometer [68] with an electrostatic energy analyser. For these experiments, a photon energy of 21.22 eV from a micro-wave driven helium discharge lamp was used.

In section 2.2 we discussed how the lowest double ionization limit can be calculated from the single ionization limit using a 'rule of thumb' for molecular valence-valence double ionization. According to Molloy *et al.* [40]

$$\varepsilon_{\mathrm{DIE}} = 2.20 \cdot \varepsilon_{\mathrm{IE}} + \frac{11.5}{r_{\mathrm{h-h}}}. \tag{4.1}$$

In this equation, $r_{\mathrm{h\text{-}h}}$ denotes the distance between the two vacancies created in the dication. One of the vacancies in the valence-valence ionized alcohol molecule is expected to be localized on the oxygen atom. It could be argued that the other vacancy should be localized on the carbon atom that lies the furthest away from the oxygen atom since the two vacancies have the same charge and therefore repel each other. On the other hand, the p-orbitals of the carbon atoms are known to be hybridized so that the electrons (and vacancies) are delocalized. Therefore, the second vacancy can be expected to be 'smeared out' over all the carbon atoms and hence one should rather use the centre of the carbon chain as the position of the second vacancy.

The single and double ionization spectra are presented in the left and right panels of figure 4.6, respectively. A general trend of lower energy for the double ionization onset as well as for the position of the first peak maximum can be observed with increasing length of the carbon chain of the alcohol molecules. In contrast, the lowest single ionization energy varies very little for the three molecules studied. The experimental and calculated energies are listed in table 4.2.

[2]Now installed in the laboratory in Stockholm.

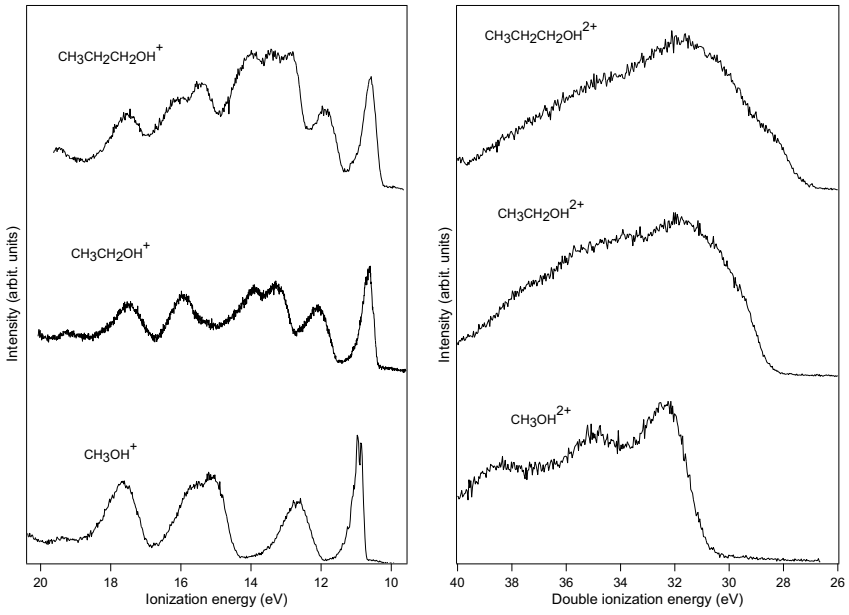

(a) Single ionization spectra *(b)* Double ionization spectra

Figure 4.6: (a) Single and (b) double ionization electron spectra of n-propyl alcohol, ethanol and methanol measured using photon energies of (a) 21.22 eV and (b) 40.814 eV. For further detail see paper III of this thesis.

As can be seen in the table, there is generally a good agreement between the calculated lowest vertical double ionization energies and the experimentally observed ones. Also, the calculated mean distance between the centre-of-mass of the carbon atoms and the oxygen atom agrees well with the values of $r_{\mathrm{h–h}}$ obtained from the 'rule of thumb' (eq. (4.1)) using experimental values of the single and double ionization energies.

4.3 Paper IV and V: Core-valence double photoionization of O_2 and CS_2

We have studied core-valence double ionization of a fairly large number of small molecules, and the results on O_2 and CS_2 are presented here. A few experimental [33, 42] and theoretical [41, 69] studies on core-valence double photoionization have been reported previously. A schematic illustration of core-valence ionization of O_2 is show in the left panel of figure 4.7.

The experiments were carried out at beamlines U49/2 PGM-1 [52, 53] and PGM-2 [54] (cf. section 3.2.2.3) of the BESSY II storage ring [49], using the magnetic bottle setup described in section 3.3.1. Core-valence spectra were

Table 4.2: *The lowest vertical experimental single ionization energies (IE_v) in comparison to the experimental and calculated onset of double ionization (DIE_{on}) and vertical double ionization energies (DIE_v). The calculated adiabatic double ionization energy for methanol is included as well. Furthermore, values for the effective distance between the electron vacancies as derived from the rule of thumb and values for the distance between the oxygen atom and the center of mass of the carbon atoms as obtained from the ab initio calculations are given (cf. paper III).*

			Alcohol		
			Methanol	Ethanol	n-propyl alcohol
IE_v	Exp	(eV)	10.96	10.64	10.49
DIE_{on}	Exp	(eV)	30.5	28.2	27.0
DIE_v	Exp	(eV)	32.1	29.6	28.2
DIE_{ad}	Calc	(eV)	28.93		
DIE_v	Calc	(eV)	32.22	29.55	28.12
r_{12}	Calc	(Å)	1.42	1.80	2.45
r_{12}	rule of thumb	(Å)	1.4	1.9	2.4

recorded at several photon energies above the 1s thresholds in O_2 and the S2p and C1s thresholds in CS_2.

The core-valence double ionization spectrum of O_2 recorded at a photon energy of 620 eV is shown in figure 4.7 together with calculated energy levels. In these calculations, which have been carried out by a collaborating research group, the core hole has not been localized. Instead a fairly large active space containing the O_2 $1\sigma_g$ and $1\sigma_u$ molecular orbitals has been used. In the figure, a small correction factor of 1.9 eV has been added to the calculated energies in order to emphasise the correspondence between the these energies and the experimental core-valence spectrum.

Assignments of the peaks in figure 4.7 based on a conventional valence photoelectron spectrum [70] and the calculations are shown in table 4.3 (cf. paper IV). The core-valence double ionization spectrum is largely similar to the valence photoelectron spectrum, which suggests that the interaction between the two vacancies in the dication is Coulombic to a large extent.

A core-valence double ionization spectrum of CS_2, where one hole is located in a S2p orbital, was recorded at a photon energy of 220 eV and is presented in figure 4.8 (labelled DIPES). A simulated spectrum is shown below the core-valence double ionization spectrum in the figure. The latter has been generated by convolving a conventional valence photoelectron spectrum [71] with two Gaussian functions separated by the S2p spin-orbit splitting of 1.27

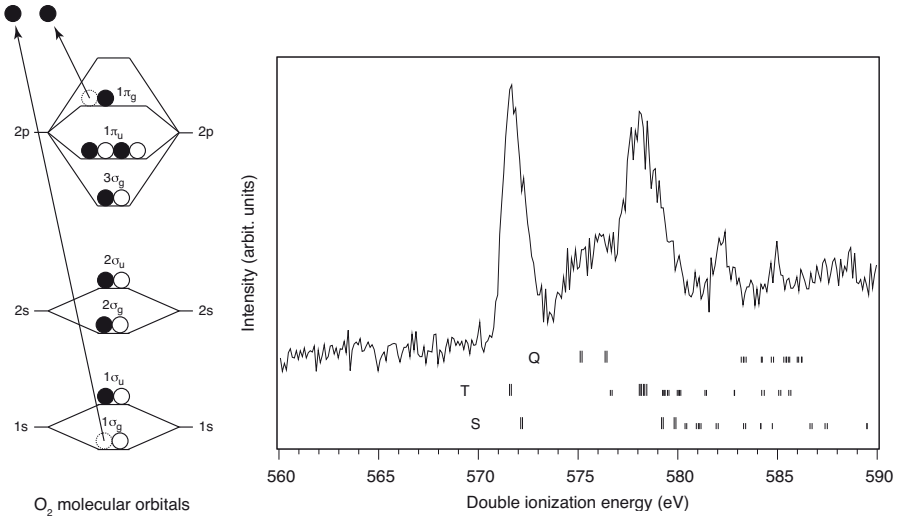

Figure 4.7: Left panel: Molecular orbitals of O_2 constructed from the atomic orbitals. In the experiment one electron was removed from a 1σ core orbital and another electron was removed from a valence orbital. Right panel: Core-valence double ionization spectrum of O_2 recorded at 620 eV. Calculated energies, arranged according to the multiplicity of the states (singlet (S), triplet (T), quintet (Q)), are included for comparison. The double ionization energies of pure two-electron ejection states are marked using tall bars and states with additional excitations or spin flips are plotted using short bars. The calculated energies have been adjusted by adding a constant value of 1.9 eV.

eV [72]. The two Gaussians have an intensity ratio of 2:1 and a full-width-at-half-maximum (FWHM) of 0.65 eV. Calculated energy levels are shown above the core-valence double ionization spectrum in the figure. In these calculations, also carried out by a collaborating research group, the core hole was kept localized on one sulphur atom. The energies of these states have been shifted by 2.79 eV in order to emphasise the correspondence to the experimental spectrum. The states have been duplicated and shifted by an additional 1.27 eV to reflect the spin-orbit coupling of the S2p hole. The simulated spectrum and the calculated energies display an obvious resemblance to the measured core-valence double ionization spectrum. Assignments of the spectral features in figure 4.8 are presented in paper V.

Figure 4.9 shows the core-valence double ionization spectrum measured for a C1s hole along with a vacancy among the valence orbitals. A photon energy of 632.7 eV was used. A simulated spectrum constructed by convolving the valence photoelectron spectrum [71] with a Gaussian function with a FWHM of 0.65 eV is shown in the lower part of the figure. The two spectra resemble each other less than in the case of $(S2p)^{-1}valence^{-1}$ double ionization (cf. figure 4.8). The carbon atom is located at the centre of the molecule where the

Table 4.3: *Experimental double ionization energies and assignments of the O_2 core-valence double ionization spectrum.*

Exp. DIEs (eV)	Assignment (leading configuration and term)		Comment
571.6	$(1\sigma_{g,u})^1...(1\pi_u)^4(1\pi_g)^1$	$^3\Pi_{g,u}$	peak max
572.3	$(1\sigma_{g,u})^1...(1\pi_u)^4(1\pi_g)^1$	$^1\Pi_{g,u}$	shoulder
575.0	$(1\sigma_{g,u})^1...(1\pi_u)^3(1\pi_g)^2$	$^5\Pi_{g,u}$	peak max
576.1	$(1\sigma_{g,u})^1...(3\sigma_g)^1$	$^5\Sigma^-_{g,u}$	weak peak max
	$(1\sigma_{g,u})^1...(1\pi_u)^3(1\pi_g)^2$	$^3\Pi_{g,u}$	
578.0	$(1\sigma_{g,u})^1...(3\sigma_g)^1$	$^3\Sigma_{g,u}$	peak max
	$(1\sigma_{g,u})^1...(1\pi_u)^3(1\pi_g)^2$	$^3\Pi_{g,u}$	
579.5	$(1\sigma_{g,u})^1...(3\sigma_g)^1$	$^1\Sigma_{g,u}$	shoulder
579.5	$(1\sigma_{g,u})^1...(1\pi_u)^3(1\pi_g)^2$	$^1\Pi_{g,u}$	shoulder
580.8			plateau
582.3			peak max
585.0	$(1\sigma_{g,u})^1...(3\sigma_g)^1$	$^5\Sigma^-_{g,u}$	peak max

$2\pi_g$ valence orbital has a nodal plane. One could anticipate that this should lower the cross section of direct double photoionization involving this orbital and C1s, but the present study does not seem to support such an interpretation.

The calculated $(C1s)^{-1}$valence^{-1} double ionization energies are marked with bars in figure 4.9. Singlet and triplet states are drawn with solid and dashed lines, respectively. No shift was added to the calculated energies in this case. The singlet-triplet splitting of the $(C1s)^{-1}\pi_g^{-1}$ is rather small (~ 0.5 eV) reflecting a small exchange interaction, while the splitting of the $(C1s)^{-1}\pi_u^{-1}$ state is considerably larger (~ 2 eV). This indicates that the carbon localized π_u^{-1} orbital collapses into the core upon C1s ionization.

4.4 Paper VI: Spectra of the triply charged ion CS_2^{3+} and selectivity in molecular Auger effects

4.4.1 Experimental details

Three different setups were used for collecting the data presented in this paper, all of them relying on the magnetic bottle spectrometer for electron detection

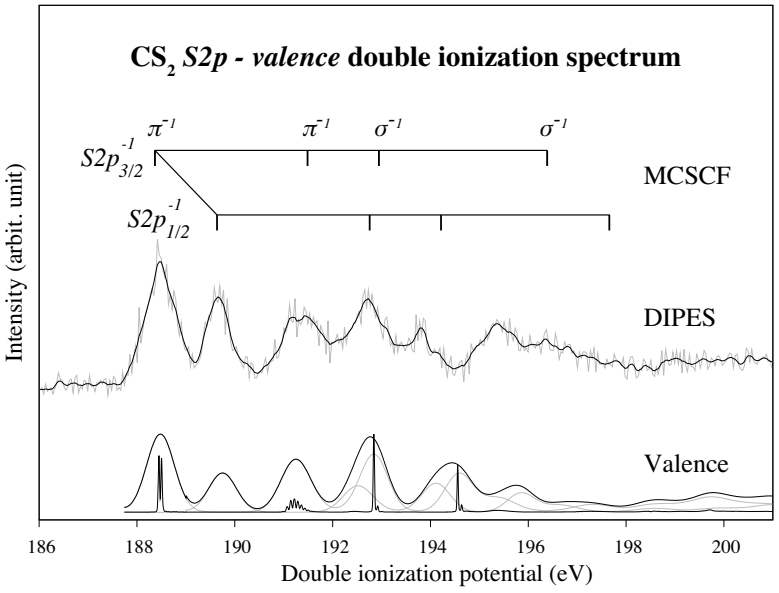

Figure 4.8: The S2p-valence double photoionization spectrum (labelled 'DIPES') of the CS_2 molecule obtained using the photon energy $h\nu = 220$ eV. The interpretation given in the figure is based on the S2p hole being either 3/2 or 1/2 coupled. A simulated spectrum (labelled 'Valence'), based on the UV photoelectron spectrum (narrow lines) constructed as described in the text and paper V is included. The first line of this spectrum is adjusted to the same energy as the corresponding line of the experimental spectrum. Calculated energies (see text and paper V) and assignments using the MCSCF method are shown above the experimental spectrum.

(cf. section 3.3.1). The first setup was the same as the one used for the experiments presented in papers I–II and IV–V of this thesis. The second setup consists of the same magnetic bottle electron spectrometer but equipped with an ion time-of-flight mass spectrometer akin to the works of Refs. [58, 59]. The latter setup was briefly described in section 3.3.4 and the timing mode will be described further below. Both setups were used at beamline U49/2 PGM 2 [54] of the BESSY II synchrotron storage ring.

The third setup was operated by our French colleagues (P. Lablanquie and coworkers) and is based on a similar magnetic bottle spectrometer design as ours, configured for electron detection only. It was mounted at beamline UE 56/2 PGM-2 [73] of BESSY II [49], which provides light at photon energies down to 63 eV. On this line, the time period between the light pulses was extended to a about 12 μs by insertion of a fast mechanical chopper [36, 57] into the light path. This device, which is basically a rotating drum with slits machined into it, was originally developed at the Photon Factory in Japan under the guidance of K. Ito. It was realized by modifying a turbo molecular

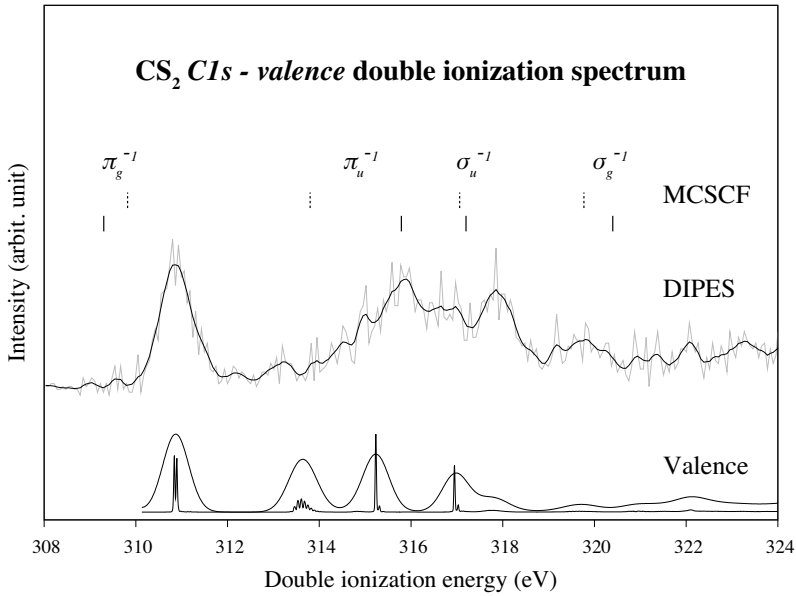

Figure 4.9: The C1s-valence double photoionization spectrum (labelled 'DIPES') of the CS_2 molecule obtained using the photon energy hν = 362.7 eV. A simulated spectrum (labelled 'Valence') based on the UV photoelectron spectrum (narrow lines) constructed as described in the text is also included. The first line of this spectrum is adjusted to the same energy as the corresponding line of the experimental spectrum. Calculated energies and assignments using the MCSCF method are shown above the experimental spectrum, where triplet states are indicated by dashed lines and singlet states with solid lines.

pump. The extension of the light pulse period makes it possible to use the ionizing light pulse as start signal (the first timing scheme described in section 3.3.2) and unambiguously associate each electron with the correct light pulse.

The second setup, which was used to detect ions in coincidence with the electrons, utilized a different timing scheme. A weak (7 V cm^{-1}) electric field was applied across the ionization region in order to extract the ions into the mass spectrometer. Since the DC field prevents the use of time delay focusing [60] in the present experiment, the width of the ionizing light beam in the plane of the mass spectrometer becomes more important. By decreasing the width of the beam to about 250 μm, which was achieved by closing the baffles at the entrance of the beamline, it became possible to identify the undissociated molecular ions and use their flight-times to identify the ionizing light pulse. The flight-times of the electrons were then referenced to the light pulse. The electric field used to extract the ions also accelerates the electrons toward the electron flight tube and in order to restore the energy resolution of

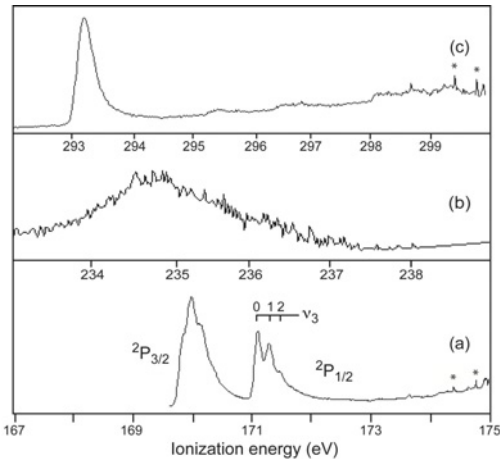

Figure 4.10: Photoelectron spectra at the inner shell edges in CS_2. (a) at 175 eV showing S2p, (b) at 243 eV showing S2s, and (c) at 300 eV showing C1s. The weak sharp features at low electron energy in (a) and (c) are mostly artifacts, but the two that occur at the same kinetic energies in the two curves (asterisks) are due to autoionization from superexcited atomic S (cf. paper VI of this thesis).

the electrons that is lost in the process, a retarding field of a similar potential difference was applied between the accelerating field and the flight tube.

The resolving power for single electrons of setup one and three can be expressed as a fixed numerical resolution $E/\Delta E$ of about 50 for electron energies above 1 eV, and a fixed width ΔE of about 20 meV at lower energies. The second setup has a lower resolution, since the ring magnet used in the ion detector creates a weaker field than the conical permanent magnet used in the electrons-only setup does. The numerical resolution ($E/\Delta E$) was about 20.

4.4.2 Results

Photoelectron spectra of the C1s, S2p and S2s edges of the CS_2 molecule are shown in figure 4.10. All these core hole states may decay to triply charged carbon disulfide states through double Auger decay. By measuring the Auger electrons in coincidence with the photoelectron, it is possible to selectively study such decays from a specific core hole state, and also for various vibrational components resolved in the $(S2p)^{-1}\ ^2P_{1/2}$ photoelectron line in figure 4.10. Furthermore, it is also possible to filter the coincidence data by putting constraints on the kinetic energies of the Auger electrons.

Figure 4.11 shows three triple ionization spectra of CS_2 produced by double Auger decays from S2p hole states. The topmost spectrum (c), where triple ionization events containing slow (< 10 eV) Auger electrons have been rejected is the most structured one of the three spectra shown. As a comparison, the middle spectrum (b) has been generated by selecting events where

one of the two Auger electrons has a kinetic energy below 4 eV. This spectrum is much less structured and we attribute the difference to Auger cascades through superexcited CS_2^{2+} states which decay to CS_2^{3+} by emission of low energy electrons, as is discussed in more detail in paper VI.

We have also studied triple ionization of carbon disulfide via $(S2p)^{-1}valence^{-1}$ (core-valence) intermediate states. Triple ionization spectra selected on several structures of this core-valence spectrum are shown in figure 4.12. The solid lines show simulated spectra from a simple model. The model assumes that each electron configuration of the triply charged ion produces a single contributing state at an energy relative to the ground state equal to the sum of the participating orbital energies taken from the photoelectron spectrum. The weight of each configuration was taken to be a product of the number of ways of choosing the electrons to be removed with a factor reflecting the extent of electron localization on one S atom. This somewhat crude model, folded with a Gaussian of 3 eV FWHM, reproduces the main features of the experimental spectra in figure 4.12 to a good approximation. In particular it shows the progressive shift to higher energies and the absence of the first (π_g^{-3}) band when a core-valence state with any other valence hole is selected. The latter phenomenon was also observed in triple ionization of krypton via intermediate core-valence states (cf. paper II).

Triple ionization via $(S2p)^{-1}$ singly charged intermediates and $(S2p)^{-1}$-$valence^{-1}$ doubly charged intermediates are examples of indirect multi-ionization via inner shells, but we have also studied triple ionization at energies below the inner shell thresholds. This was done by two different methods. First, by detecting ions in coincidence with the electrons and, second, by using the mechanical chopper technique. The latter setup allows for high-resolution detection of triple coincidence events where all three electrons have low kinetic energy. A spectrum recorded with this technique at a photon energy of 63 eV shows a sharp peak at 53.1 ± 0.1 eV, which agree well with the value of 53.6 ± 0.5 eV reported by Newton [17] and is slightly below the value reported in Ref. [76].

The ion setup was also used to study the relative yield of triple ionization and the branching ratios of the dissociations of the triply ionized molecule. The results are listed in table 4.4. As can be seen, the values show that the overall abundance of triple ionization increases with photon energy, from about 1% at 100 eV to over 20% above the S2p and C1s edges. Within the overall triple ionization, formation of stable CS_2^{3+} is a constant fraction of 5% of the total triple ionization, at all energies. The major dissociation pathways in triple photoionization are atomizations, to $S^+ + C^+ + S^+$, to $S^+ + S^{2+} + C$ and to $C^+ + S^{2+} + S$. None of the present measurements can determine, however, whether the dissociations happen directly from nascent triply ionized molecules, or through dissociation of superexcited singly or doubly ionized intermediates.

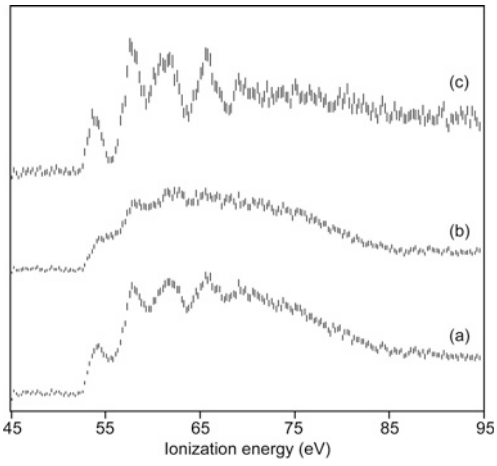

Figure 4.11: Spectra of triply ionized CS_2 produced by the double Auger decays from S2p ionized hole states of CS_2^+. Spectrum (a) includes all Auger pairs; spectrum (b) is from pairs with one electron of energy below 4 eV and spectrum (c) is from pairs where all the Auger electrons have at least 10 eV energy.

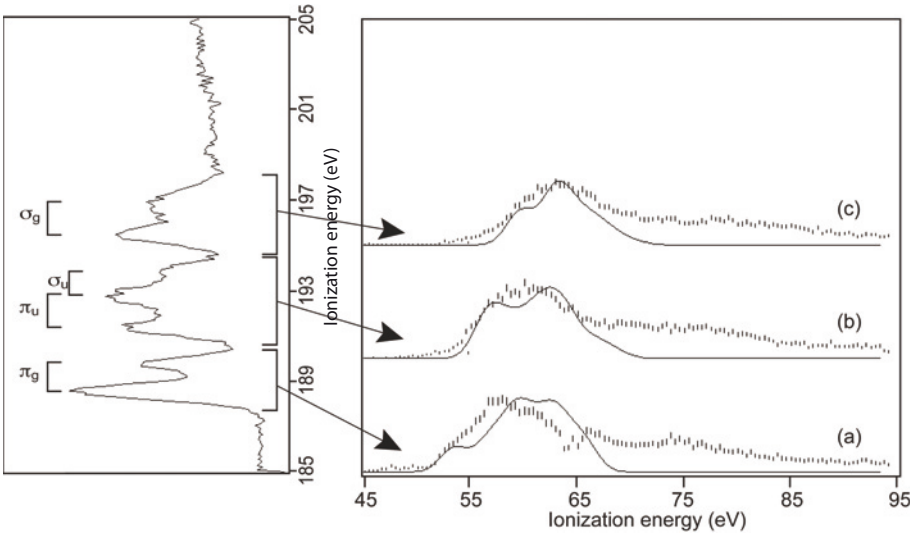

Figure 4.12:
Formation of CS_2^{3+} by Auger decay via selected core-valence states of CS_2^{2+} (left panel) produced by double photoionization at 230 eV photon energy. The selected energy ranges within the core valence spectrum are shown to the right of the curve in the left hand panel, while the proposed valence orbital hole identities are shown to the left. Right panel: Triple ionization spectrum from (a) from $S2p^{-1}\pi_g^{-1}$, (b) from $S2p^{-1}\pi_u^{-1}$ and $S2p^{-1}\sigma_u^{-1}$, and (c) from $S2p^{-1}\sigma_g^{-1}$. The solid lines show simulated spectra from a simple model (cf. paper VI).

Table 4.4: *Relative intensities and branching ratios of triple ionization and stable triply charged ions at five different photon energies; 164.6 eV is the peak position of a representative pre-edge resonance (see e.g. Ref. [74] for an absorption spectrum); 180 eV is above the S2p ionization edges (169.934 and 171.075 eV [72]); 236 eV is on the high-energy tail of the S2s edge (234.85 eV [this paper]). There is no great change at the C1s edge (293.1 eV [75]). ΣI represents the number of absorptions producing ionization, while ΣDI and ΣTI are the numbers of double and triple ionization events, both dissociative and non-dissociative.*

Photon Energy	100 eV	150 eV	164.6 eV	180 eV	236 eV
			Relative yields		
CS_2^{3+} / CS_2^{2+}	0.01	0.025	0.05	0.04	0.07
CS_2^{3+} / ΣTI	0.04	0.045	0.05	0.05	0.04
ΣTI / ΣI	0.011	0.037	0.053	0.12	0.24
ΣDI / ΣI	0.18	0.31	0.43	0.65	0.76
			Branching ratios in triple ionization		
CS_2^{3+}	4%	5%	3.1%	4.7%	4.3%
$S^+ + CS^{2+}$	20%	6%	3.5%	5%	6.5%
$S^{2+} + CS^+$	-	5%	7.5%	6.9%	5.7%
$S^{2+} + S^+$	35%	32%	37%	29%	34.5%
$C^+ + S^{2+}$	-	27%	6%	24%	46.5%
$C^+ + 2S^+$	41%	30%	47%	27%	4.2%

5. Outlook

The study of multi-ionization processes using the magnetic bottle time-of-flight spectrometer is a fairly recent and rapidly progressing research field, with several research groups around the world pushing the technique forward. Only five years have passed since the first synchrotron based experiments were carried out [32], and paved the way for a wide range of experiments. The recent introduction of a mechanical chopper [57, 36] has widened the range of possible experiments even further. While this thesis is being printed, the Uppsala-Oxford research team is implementing a mechanical chopper with a different, and less costly design compared to the one constructed by Ito *et al.* [57]. The new chopper will also be synchronized with the synchrotron storage ring.

New possibilities are opened up by the access to femtosecond lasers as ionizing lightsource. Several opportunities are being tried out or are under construction.

- Multi-photon ionization of atoms and molecules. Successful experiments have already been carried out in the laboratory in Stockholm [77].
- Two-color pump-probe ionization experiments using electron detection. Interesting results on the fragmetation dynamics of e.g. acetone [77] have already been found.
- High harmonic generation. Ongoing projects in Stockholm and Uppsala aim for pulsed soft x-ray sources that can be used in the local laboratories.

Free Electron Lasers (FELs) represent an increasingly important kind of light source with extremely high brightness in the vacuum ultraviolet and x-ray spectral region. This provides an opportunity to study non-linear effects and perform time resolved experiments. In this respect the FEL is similar to the femtosecond lasers providing light in the infrared–ultraviolet spectral range mentioned above. However, the high energy of the photons generated in the FEL opens up new fields such as few-photon multi-ionization, which bridges the gap between the single-photon multi-ionization experiments discussed in this thesis and the multi-photon ionization experiments that can be carried out using lasers in the home laboratories. With respect to the possibilities offered by FELs, the Uppsala-Stockholm team is currently developing a dedicated magnetic bottle electron spectrometer to be combined with the so-called CFEL multipurpose experimental chamber CAMP of the collaborating group of Joachim Ullrich at the Max Planck Institut für Kernphysik in Heidelberg.

6. Sammanfattning på svenska

Den här avhandlingen presenterar experiment på atomer och små molekyler där vi undersökt hur elektronerna som omger atomkärnorna interagerar med varandra. För att göra detta kan man använda spektroskopiska metoder. Spektroskopi jämförs ibland med mikroskopi. Båda kan ge en inblick i system som är så små att de är osynliga för blotta ögat. Men till skillnad från mikroskopi så är spektroskopi inte en avbildande teknik. I stället studerar man hur en egenskap, t ex hur mycket ljus som absorberas, varierar med t ex våglängden. Det finns en stor mängd olika spektroskopiska tekniker som används bland annat för att studera grundläggande fysik eller för att karaktärisera prover.

Vi har använt en form av elektronspektroskopi vars grundläggande idé är att mäta rörelseenergin på elektroner som slagits loss, joniserats, från ett prov. Själva jonisationsprocessen åstadkoms genom att belysa provet med fotoner med hög energi. Vi har använt 'ljus' som har högre energi än synligt ljus och mindre än röntgenstrålning. Man brukar dela in det här spektrala området i ultraviolett-, vakuumultraviolett- och mjukröntgenstrålning. Vi har använt ljuspulser med fotoner av de två senare typerna.

När en foton absorberas av en atom eller en molekyl finns det flera olika processer som kan leda till att elektroner sänds ut (emitteras). Joniserade molekyler kan dessutom brytas isär, dvs dissociera. Vi är intresserade av processer där flera elektroner emitteras och för att kunna skilja på händelser från skilda processer har vi mätt elektronerna i koincidens. Detta innebär att alla partiklar (elektroner och eventuellt även joner) som skapats av samma ljuspuls samlas in och detekteras. Alla partiklar som detekteras under ett visst tidsintervall (ca 5–10 mikrosekunder) antas härröra från samma jonisation*shändelse*. På så vis kan man enkelt skilja på t ex enkeljonisation och dubbeljonisation eftersom man detekterar en elektron i det första fallet och två elektroner i det andra. Tekniken förutsätter förstås att bara en jonisationshändelse sker under tidsfönstret och att partiklarna detekteras med hög effektivitet. I våra experiment har vi använt en koincidensmetod som bygger på 'time-of-flight', dvs flygtid, med en magnetisk flaska [25, 56]. Genom att mäta hur lång tid det tar för elektronerna att åka genom ett rör på ca två meter kan man räkna ut vilken rörelseenergi de har och därmed räkna ut hur mycket energi det behövs för att slå loss dem från provet. Den magnetiska flaskan utmärks av en mycket hög insamlingseffektivitet; nästan hela rymdvinkeln täcks för elektroner med rörelseenergi mellan noll och flera hundra elektronvolt.

Dubbelfotojonisation, där en elektron från en inre orbital och en elektron från en valensorbital slås ut av en foton, har inom ramen för avhandlingen studerats för Kr, O_2 och CS_2. Processen är schematiskt illustrerad i figur 4.7. Dessa experiment har utförts med mjukröntgenljuspulser på synkrotronljusanläggningen BESSY II [49] i Berlin. Ett antal olika tekniker för att bestämma flygtiderna har använts, t ex genom att utnyttja [32] sekundära Augersönderfall [12] med välbestämda, höga rörelseenergier, samt genom att detektera joner i koincidens med elektronerna [35]. Dessa 'core-valens'-dubbeljonisationsspektra av molekylerna har tolkats med hjälp av valensfotoelektronspektra och kvantkemiska beräkningar. Dubbeljonisationsspektra där en elektron tagits bort från O1s i O_2 eller från S2p i CS_2 visar sig vara tämligen lika motsvarande valensfotoelektronspektra, vilket tyder på att interaktionen mellan de två hålen i den dubbelladdade jonen till största delen har Coulombisk karaktär. På C1s-kanten är dubbeljonisationsspektrumet mindre likt valensfotoelektronspektrumet. Kvantkemiska beräkningar visar att singlett/triplett-uppspaltningen är ganska liten då innerskalsvakansen är belägen i S2p och något större då den är belägen i C1s. Intensiteten för de beräknade tillstånden varierar också i större grad för $(C1s)^{-1}$- än för $(S2p)^{-1}$-$valens^{-1}$ dubbeljonisationsspektrumet.

Genom att mäta de emitterade elektronerna i koincidens är det möjligt att välja ut enskilda jonisationskanaler. Detta har använts för att studera hur trippeljoniserat koldisulfid (CS_2^{3+}) bildas genom dubbelaugersönderfall från CS_2^+-molekyler med en innerskalsvakans och genom enkelaugersönderfall från $(S2p)^{-1}valens^{-1}$-joniserat CS_2. Dubbelfotojonisation av krypton till $3d^{-1}4p^{-1}$-tillstånd har studerats och vi har observerat en viss selektivitet i dessas Augersönderfall till trippeljoniserade tillstånd. Vidare har vi studerat hur Kr^+ med en vakans i 3d sönderfaller till $4p^{-3}$-tillstånd i Kr^{3+}. Dessa dubbelaugersönderfall visade sig främst ske stegvis via exciterade mellantillstånd i Kr^{2+}. Vi har identifierat sju sådana mellantillstånd.

Förutom de synkrotronljusbaserade experimenten har valens-valens-dubbelfotojonisation av en serie alkoholmolekyler studerats med hjälp av en pulsad vakuumultraviolet ljuskälla som finns tillgänglig i vårt laboratorium i Stockholm. I denna används en sk hålkatodsurladdning för att skapa korta urladdningar i en kapillär fylld med en heliumgas [25, 46, 44]. En empirisk regel [40] för att uppskatta dubbeljonisationströskeln har testats experimentellt för tre alkoholmolekyler. De erhållna resultaten har även jämförts med kvantkemiska beräkningar.

7. Acknowledgements

First of all I would like to thank my supervisors Raimund Feifel and Jan-Erik Rubensson for all their support during these years. I would also like to thank John Eland, who has been very closely involved in all stages of the work. Furthermore, he has worked his magic with the equipment and has been an inspiration to us all. I want to thank Leif Karlsson, with whom I have worked very closely. It has been a privilege. Furthermore, I want to thank Pelle Linusson, for his friendship and for sharing his insights into coincidence spectrocopy, Johan Forsberg, who has been a good friend and discussion partner, and Anders Olsson, who always have been willing to give a helping hand. I am most indebted to all of you.

Many more people have been involved in the development of the time-of-flight setup. I would especially like to thank Isak Bakken, Pernilla Andersson and Tomasz Kloda. The Stockholm group as a whole is acknowledged for the very welcoming atmosphere.

During my stay in Berlin I met many warm and forthcoming fellow physicists. In particular I would like to thank Emad Aziz, Stefan Eisebitt and Gerd Reichardt for all their help.

In the Uppsala group, I would like to thank Joakim Andersson and Calle Englund, who taught me nearly all the lab-work I know, my fellow PhD students Filip Heijkenskjöld, Johan Vegelius, Johan Söderström, Anders Modin, Johan Gråsjö, Lage Hedin, Håkan Hollmark and Paw Kristiansen, and others contributing to this work.

The financial assistance from C. Henschens stipendiestiftelse, managed by Upland's Nation, and Wilgott Stenholms stipendiestiftelse, which is managed by Uppsala University and which supported my 6 months stay at the BESSY II facility in Berlin, is gratefully acknowledged.

Finally, I want to thank my friends and family for their support and encouragement.

8. Credits

Reprints of the papers were made with permission from the publishers. Figures 1.3 and 4.5 contains elements which are part of the public domain. Figure 1.1 is based on course material published in Ref. [78]. Figures 3.2 and 3.3 are based on figures in Ref. [79] and have been modified with the permission of their original creator. Figure 3.4 is a part of the documentation of the U49/2 PGM 2 beamline at BESSY II. Credit is due to Ref. [50].

The figures and tables in chapter 4, which have previously been published in journals are reproduced here with the kind permission of the publishers. In particular, the right panel of figure 4.7, table 4.3 and figure 4.6 are reprinted with the permission of Physical Review A. Copyright 2008, 2008 and 2009, respectively, of the American Physical Society. Table 4.4, and figures 4.12, 4.11 and 4.10 are reprinted with permission from the Journal of Chemical Physics. Copyright 2010, American Institute of Physics.

Bibliography

[1] J. Sjöström, in *Kosmos*, vol. 85, pp. 103–123 (Svenska fysikersamfundet, 2008), editor: L. Karlsson.

[2] B. Bröcker. *Atlas de la physique atomique et nucléaire* (Librarie Générale Française/Deutscher Taschenbuch Verlag, 2001).

[3] J. Dalton. *New System of Chemical Philosophy* (R. Bickerstaff, Strand, London, 1808).

[4] A.-L. de Lavoisier. *Traité élémentaire de chimie* (Cuchet, 1789).

[5] B. C. Bransden and C. J. Joachain. *Physics of Atoms and Molecules* (Prentice Hall/Pearson Education, 2003).

[6] H. Geiger and E. Marsden. *Proc. R. Soc. London, Ser. A* **82**, no. 557, pp. 495–500 (1909). doi:10.1098/rspa.1909.0054.

[7] L. D. Landau and E. M. Lifshitz (swe: Lifšic). *Quantum mechanics: non-relativistic theory* (Pergamon Press, London, 1958).

[8] S. Andersson, F. Bruhn, J. Hedman, L. Karlsson, S. Lunell, K. Nilson and J. Wall. *Atom- och molekylfysik* (Fysiska institutionen, 2001).

[9] R. P. Feynman, R. B. Leighton and M. Sands. *The Feynman lectures on physics; Quantum mechanics*, vol. 3 (Addison-Wesley, 1966).

[10] L. Meitner. *Z. Phys.* **17**, no. 54 (1923).

[11] P. Auger. *J. Phys. Radium* **6**, no. 6, pp. 205–208 (1925). doi:10.1051/jphysrad:0192500606020500.

[12] W. Mehlhorn. *J. Electron. Spectrosc. Relat. Phenom.* **93**, no. 1-3, pp. 1 – 15 (1998). doi:10.1016/S0368-2048(98)00153-4.

[13] T. A. Carlson and M. O. Krause. *Phys. Rev. Lett.* **14**, no. 11, pp. 390–392 (1965). doi:10.1103/PhysRevLett.14.390.

[14] J. H. D. Eland, in *Adv. Chem. Phys.*, vol. 141, chap. 3, pp. 103–151 (Wiley, Hoboken, New Jersey, 2009), editor: Stuart A. Rice.

[15] J. H. D. Eland, in *Vacuum Ultraviolet Photoinization and Photodissociation of Molecules and Clusters*, chap. 6, pp. 297–343 (World Scientific, Singapore, 1991), editor: C. Y. Ng.

[16] J. J. Thompson. *Rays of positive Electricity* (Cambridge University Press, 1921), 2 edn.

[17] A. S. Newton. *J. Chem. Phys.* **40**, no. 2, pp. 607–608 (1964). doi:10.1063/1.1725172.

[18] A. S. Newton and A. F. Sciamanna. *J. Chem. Phys.* **40**, pp. 718–723 (1964). doi:10.1063/1.1725195.

[19] R. G. Cooks, D. T. Terwilliger and J. H. Beynon **61**, pp. 1208–1213 (1974). doi:10.1063/1.1681995.

[20] M. Thompson, M. D. Baker, A. Christie and J. F. Tyson. *Auger electron spectroscopy* (Wiley, 1985).

[21] T. Åberg. *Physica Scripta* **1992**, no. T41, p. 71 (1992).

[22] P. Lablanquie, J. H. D. Eland, I. Nenner, P. Morin, J. Delwiche and M. J. Hubin-Franskin. *Phys. Rev. Lett.* **58**, no. 10, pp. 992–995 (1987). doi:10.1103/PhysRevLett.58.992.

[23] S. D. Price and J. H. D. Eland. *J. Electron. Spectrosc. Relat. Phenom.* **52**, pp. 649 – 660 (1990). doi:10.1016/0368-2048(90)85054-D.

[24] K. Okuyama, J. H. D. Eland and K. Kimura. *Phys. Rev. B* **41**, no. 9, pp. 4930–4935 (1990). doi:10.1103/PhysRevA.41.4930.

[25] J. H. D. Eland, O. Vieuxmaire, T. Kinugawa, P. Lablanquie, R. I. Hall and F. Penent. *Phys. Rev. Lett.* **90**, no. 5, p. 053003 (2003). doi: 10.1103/PhysRevLett.90.053003.

[26] R. I. Hall, A. G. McConkey, L. Avaldi, K. Ellis, M. A. MacDonald, G. Dawber and G. C. King. *J. Phys. B* **25**, no. 6, p. 1195 (1992).

[27] R. I. Hall, G. Dawber, A. McConkey, M. A. MacDonald and G. C. King. *Phys. Rev. Lett.* **68**, no. 18, pp. 2751–2754 (1992). doi:10.1103/PhysRevLett.68.2751.

[28] J. Ullrich, R. Moshammer, R. Dörner, O. Jagutzki, V. Mergel, H. Schmidt-Böcking and L. Spielberger. *J. Phys. B* **30**, no. 13, p. 2917 (1997).

[29] R. Dörner, V. Mergel, O. Jagutzki, L. Spielberger, J. Ullrich, R. Moshammer and H. Schmidt-Böcking. *Phys. Rep.* **330**, no. 2-3, pp. 95 – 192 (2000). doi: 10.1016/S0370-1573(99)00109-X.

[30] G. C. King and L. Avaldi. *J. Phys. B* **33**, no. 16, p. R215 (2000).

[31] J. Ullrich, R. Moshammer, A. Dorn, R. Dörner, L. P. H. Schmidt and H. Schmidt-Böcking. *Rep. Prog. Phys.* **66**, no. 9, p. 1463 (2003).

[32] F. Penent, J. Palaudoux, P. Lablanquie, L. Andric, R. Feifel and J. H. D. Eland. *Phys. Rev. Lett.* **95**, pp. 083002–4 (2005).

[33] Y. Hikosaka, T. Aoto, P. Lablanquie, F. Penent, E. Shigemasa and K. Ito. *Phys. Rev. Lett.* **97**, pp. 053003–4 (2006).

[34] Y. Hikosaka, P. Lablanquie, F. Penent, T. Kaneyasu, E. Shigemasa, J. H. D. Eland, T. Aoto and K. Ito. *Phys. Rev. B* **76**, no. 3:032708 (2007). doi: 10.1103/PhysRevA.76.032708.

[35] J. H. D. Eland, P. Linusson, L. Hedin, E. Andersson, J.-E. Rubensson and R. Feifel. *Phys. Rev. B* **78**, p. 063423 (2008).

[36] Y. Hikosaka, P. Lablanquie, F. Penent, T. Kaneyasu, E. Shigemasa, R. Feifel, J. H. D. Eland and K. Ito. *Phys. Rev. Lett.* **102**, no. 1, p. 013002 (2009). doi: 10.1103/PhysRevLett.102.013002.

[37] L. Partanen. *Auger cascade processes in xenon and krypton studied by electron and ion spectroscopy*. Ph.D. thesis, University of Oulu (2007).

[38] J. S. Briggs and V. Schmidt. *J. Phys. B* **33**, no. 1, pp. R1–R48 (2000).

[39] B. P. Tsai and J. H. D. Eland. *International Journal of Mass Spectrometry and Ion Physics* **36**, no. 2, pp. 143 – 165 (1980). doi:10.1016/0020-7381(80)80064-7.

[40] R. D. Molloy, A. Danielsson, L. Karlsson and J. H. Eland. *Chem. Phys.* **335**, no. 1, pp. 49 – 54 (2007). doi:10.1016/j.chemphys.2007.03.016.

[41] H. D. Schulte, L. S. Cederbaum and F. Tarantelli. *J. Chem. Phys.* **105**, no. 24, pp. 11108–11133 (1996). doi:10.1063/1.472912.

[42] Y. Hikosaka, T. Kaneyasu, E. Shigemasa, P. Lablanquie, F. Penent and K. Ito. *J. Chem. Phys.* **127**, pp. 044305–4 (2007).

[43] M. Stenrup. *Quantum mechanical studies of ionization and electron transfer in diatomic systems : O_2 and $H^+ + H^-$*. Licentiate thesis, Kungliga Tekniska Högskolan, School of Biotechnology, Stockholm (2008).

[44] J. H. D. Eland. *J. Electron. Spectrosc. Relat. Phenom.* **144-147**, pp. 1145 – 1150 (2005). doi:10.1016/j.elspec.2005.01.153.

[45] O. Vieuxmaire. *Double photoionisation of rare gases*. Ph.D. thesis, Oxford University (2002).

[46] P. Choi and M. Favre. *Rev. Sci. Instrum.* **69**, no. 9, pp. 3118–3122 (1998). doi: 10.1063/1.1149069.

[47] http://www.lightsources.org (Available March 2010).

[48] D. T. Attwood. *Soft x-rays and Extreme Ultraviolet Radiation* (Cambridge University Press, 1999).

[49] http://www.bessy.de (Available March 2010).

[50] 'U49/2-PGM-2 (BTU-Cottbus)'. Online beamline documentation (2003) http://www.bessy.de/upload/bitpdfs/ID_15_2.pdf.

[51] W. B. Peatman. *Gratings, mirrors and slits: beamline design for soft X-ray synchrotron radiation sources* (Gordon & Breach, Amsterdam, 1997).

[52] R. Follath and F. Senf. *Nucl. Instrum. Methods A* **390**, pp. 388–394 (1997).

[53] K. J. S. Sawhney, F. Senf and W. Gudat. *Nucl. Instrum. Methods A* **467-468**, pp. 466–469 (2001).

[54] K. J. S. Sawhney, F. Senf, M. Scheer, F. Schafers, J. Bahrdt, A. Gaupp and W. Gudat. *Nucl. Instrum. Methods A* **390**, pp. 395–402 (1997).

[55] F. A. Jenkins and H. E. White. *Fundamentals of optics* (McGraw-Hill, 1976), 4 edn.

[56] P. Kruit and F. H. Read. *J. Phys. E* **16**, no. 4, pp. 313–324 (1983).

[57] K. Ito, F. Penent, Y. Hikosaka, E. Shigemasa, I. H. Suzuki, J. H. D. Eland and P. Lablanquie. *Rev. Sci. Instrum.* **80**, no. 12:123101 (2009). doi: 10.1063/1.3258200.

[58] J. H. D. E. Eland and R. Feifel. *Chem. Phys.* **327**, pp. 85–90 (2006).

[59] R. Feifel, J. H. D. Eland, L. Storchi and F. Tarantelli. *J. Chem. Phys.* **125**, no. 19:194318 (2006). doi:10.1063/1.2386154.

[60] W. C. Wiley and I. H. McLaren. *Rev. Sci. Instrum* **26**, no. 12, p. 1150 (1955).

[61] S. Svensson, B. Eriksson, N. Mårtensson, G. Wendin and U. Gelius. *J. Electron. Spectrosc. Relat. Phenom.* **47**, pp. 327 – 384 (1988). doi:10.1016/0368-2048(88)85020-5.

[62] P. Bolognesi, L. Avaldi, M. C. A. Lopes, G. Dawber, G. C. King, M. A. MacDonald, C. Villani and F. Tarantelli. *Phys. Rev. B* **64**, no. 1, p. 012701 (2001). doi:10.1103/PhysRevA.64.012701.

[63] E. J. McGuire. *Phys. Rev. B* **11**, no. 1, pp. 17–25 (1975). doi:10.1103/PhysRevA.11.17.

[64] J. Jauhiainen, A. Kivimaki, S. Aksela, O.-P. Sairanen and H. Aksela. *J. Phys. B* **28**, pp. 4091–4100 (1995). doi:10.1088/0953-4075/28/18/012.

[65] L. Partanen, M. Huttula, H. Aksela and S. Aksela. *J. Phys. B* **40**, no. 19, pp. 3795–3805 (2007).

[66] I. P. Grant. *Methods in Computational Chemistry*, vol. 2 (Plenum Press, 1988).

[67] *Nomenclature of Organic Chemistry, Sections A, B, C, D, E, F, and H. (Blue Book)* (Oxford: Pergamon, 1979) ISBN 0-08022-3699.
IUPAC Secretariat, PO Box 13757, Research Triangle Park, NC 27709-3757, USA.

[68] Phelix photoelectron spectrometer, Gammadata-Scienta instruments, Uppsala, Sweden.

[69] H. D. Schulte, L. S. Cederbaum and F. Tarantelli. *Phys. Rev. B* **60**, no. 3, pp. 2047–2062 (1999). doi:10.1103/PhysRevA.60.2047.

[70] P. Baltzer, B. Wannberg, L. Karlsson, M. C. Göthe and M. Larsson. *Phys. Rev. B* **45**, p. 4374 (1992).

[71] L. Hedin, J. H. D. Eland, L. Karlsson and R. Feifel. *Chem. Phys.* **355**, pp. 55–61 (2009).

[72] H. Wang, M. Bässler, I. Hjelte, F. Burmeister and L. Karlsson. *J. Phys. B* **34**, no. 9, p. 1745 (2001).

[73] K. J. S. Sawhney, F. Senf, M. Scheer, F. Schäfers, J. Bahrdt, A. Gaupp and W. Gudat. *Nucl. Instrum. Methods A* **390**, no. 3, pp. 395 – 402 (1997). doi: 10.1016/S0168-9002(97)00402-6.

[74] L. Hedin, J. H. D. Eland, L. Karlsson and R. Feifel. *J. Phys. B* **42**, no. 8, p. 085102 (2009).

[75] C. J. Allan, U. Gelius, D. A. Allison, G. Johansson, H. Siegbahn and K. Siegbahn. *J. Electron. Spectrosc. Relat. Phenom.* **1**, pp. 131–151 (1972). doi: 10.1016/0368-2048(72)80027-6.

[76] D. Mathur and F. M. Harris. *Mass Spectrometry Reviews* **8**, no. 4, pp. 269–291 (1989).

[77] T. Kloda. Licentiate thesis (to be presented at Stockholm University 2010).

[78] Course material from http://crab0.astr.nthu.edu.tw/~hchang/ga2/ch07-01.htm (Available March 2010).

[79] J. Forsberg. *In Situ Soft X-ray Spectroscopies Applied to Atmospheric Corrosion And Related Systems*. Ph.D. thesis, Uppsala University, Department of Physics and Materials Science (2009).

Acta Universitatis Upsaliensis

Digital Comprehensive Summaries of Uppsala Dissertations from the Faculty of Science and Technology 743

Editor: The Dean of the Faculty of Science and Technology

A doctoral dissertation from the Faculty of Science and Technology, Uppsala University, is usually a summary of a number of papers. A few copies of the complete dissertation are kept at major Swedish research libraries, while the summary alone is distributed internationally through the series Digital Comprehensive Summaries of Uppsala Dissertations from the Faculty of Science and Technology. (Prior to January, 2005, the series was published under the title "Comprehensive Summaries of Uppsala Dissertations from the Faculty of Science and Technology".)

Distribution: publications.uu.se
urn:nbn:se:uu:diva-122811

ACTA
UNIVERSITATIS
UPSALIENSIS
UPPSALA
2010